

## EXPERIMENTAL NEAR-INFRARED SPECTROSCOPY OF POLYCYCLIC AROMATIC HYDROCARBONS BETWEEN 0.7 AND 2.5 $\mu\text{m}$

A. L. MATTIODA,<sup>1,2</sup> D. M. HUDGINS,<sup>1</sup> AND L. J. ALLAMANDOLA<sup>1</sup>

Received 2005 February 3; accepted 2005 March 30

### ABSTRACT

The near-infrared (NIR) spectra and absolute band strengths of 27 polycyclic aromatic hydrocarbon (PAH) cations and anions ranging in size from  $\text{C}_{14}\text{H}_{10}$  to  $\text{C}_{50}\text{H}_{22}$  are reported. The spectra of all the ionized PAHs we have studied to date have strong, broad absorption bands in the NIR. This work shows that ionized PAHs have significant absorption bands at wavelengths longer than predicted by the current astronomical models that consider PAHs in their treatment of the radiation balance of the interstellar medium. Two implications are (1) that ionized/open-shell interstellar PAHs should add weak, broadband structure to the NIR portion of the interstellar extinction curve and (2) that UV-poor radiation fields can pump the PAH emission bands, provided ionized/open-shell PAHs are present.

*Subject headings:* astrochemistry — dust, extinction — ISM: general — ISM: molecules — molecular data

### 1. INTRODUCTION

Ground-, air-, and space-based observations have shown that most interstellar and circumstellar objects in the Galaxy and many extragalactic objects emit a spectrum originating from a family of highly vibrationally excited polycyclic aromatic hydrocarbon (PAH) molecules (e.g., Haas et al. 1995; Cox & Kessler 1999 and references therein). The PAH bands dominate the mid-IR spectrum of many, if not most, of these objects. Thanks to a decade of focused laboratory efforts dedicated to understanding their IR spectral properties under interstellar conditions (Mattioda et al. 2003; Hudgins et al. 2000; Szczepanski et al. 1995a; Oomens et al. 2003; Kim & Saykally 2002 and references therein), these features are now being used as new diagnostics of the chemical and physical conditions in a variety of astronomical objects and environments, including planetary and reflection nebulae, the diffuse ISM, normal galaxies, starburst regions in galactic nuclei, and many other objects (e.g., Allamandola et al. 1999; Pech et al. 2002; Verstraete et al. 2001; Peeters et al. 2002, 2004; Hony et al. 2001; van Kerckhoven et al. 2000; Moutou et al. 2000; Roussel et al. 2001). Furthermore, in addition to probing local conditions, given the presence of the PAH emission spectrum in many extragalactic spectra, it can serve as an important tracer of carbon and molecular evolution in the universe (e.g., Lagache et al. 2004). Finally, and most relevant for this work, PAHs also moderate the radiation field, lending structure to the extinction curve and efficiently converting optical photons into mid-infrared photons.

Although several interstellar processes such as UV photon absorption, electron recombination, and hydrogen addition can pump PAHs into highly vibrationally excited states, the mechanism that most efficiently excites the emission from the majority of objects measured to date is that of optical photon absorption. Over the past 15 years, while a significant amount of laboratory and theoretical work has been directed toward understanding the global infrared spectral properties of PAHs under conditions appropriate to the emission zones (i.e., cold, isolated molecules in their neutral and ionized forms), significantly less has been

directed toward understanding their overall UV-visible and near-IR spectral properties. For these electronic transitions, most experimental effort has focused on testing the hypothesis that PAHs are responsible for some of the discrete diffuse interstellar bands (DIBs) that span the visible and near-IR spectral regions (Salama et al. 1996; Bréchignac & Pino 1999; Biennier et al. 2003).

As the IR emission bands were found to be associated with UV-rich objects and the then-available electronic spectra of PAHs showed that PAHs were very strong UV absorbers, it was generally assumed that the interstellar emission bands were pumped by UV photons in spite of occasional early reports that lower energy photons were needed to account for their luminosity (e.g., Aitken & Roche 1983). To better constrain this aspect of the emission process and provide a test of the PAH hypothesis, Uchida et al. (1998) carried out a detailed, careful study of the emission from reflection nebulae pumped by different stellar types. They showed that the interstellar infrared emission bands could be pumped by less energetic photons as well. Given the paucity of experimental data on the overall electronic spectral properties of PAHs taken under appropriate astronomical conditions, this result raised questions about the validity of the PAH model.

Understanding how PAHs might moderate the interstellar radiation field as well as using them as probes of the interstellar medium has been severely limited by the lack of complete UV/visible/near-IR spectroscopic data measured in the laboratory under conditions relevant to the emission regions, where they are isolated (i.e., individual molecules in the gas phase) and likely to be ionized. There are several studies of the UV and visible spectroscopic properties of PAHs relevant to the astrophysical problem. The general electronic spectroscopic properties of only a few PAH ions trapped in various glasses (Kasha 1948; Hoijtink 1959; Hoijtink et al. 1960; Shida & Iwata 1973) and rare gas matrices (Andrews & Blankenship 1981; Andrews et al. 1985) were available when it was recognized that PAHs might be widespread throughout the interstellar medium. These have been followed by experimental and theoretical studies on many PAHs, motivated in large part to address the astrophysical problem (e.g., Hirata et al. 2003, references 22–49). However, very little is known about the overall near-IR spectroscopic properties of many PAHs. To start to remedy this situation for so important

<sup>1</sup> NASA Ames Research Center, Moffett Field, CA 94035-1000.

<sup>2</sup> SETI Institute, 515 North Whisman Road, Mountain View, CA 94043.

an interstellar species, we have undertaken an ongoing, systematic study of the near-infrared (NIR) spectroscopic properties of PAH ions isolated in argon matrices in parallel to our mid-infrared work. The results of this investigation are summarized here.

Nearly all ionized PAHs we have studied to date have strong, broad absorption bands in the NIR arising from electronic transitions. The NIR spectra and absolute band strengths of 12 PAHs ( $C_{14}H_{10}$  to  $C_{24}H_{12}$ ) in the  $14000\text{--}9000\text{ cm}^{-1}$  ( $0.7\text{--}1.1\text{ }\mu\text{m}$ ) region and 15 PAHs ( $C_{18}H_{22}$  to  $C_{50}H_{22}$ ) in the  $14000\text{--}4000\text{ cm}^{-1}$  ( $0.7\text{--}2.5\text{ }\mu\text{m}$ ) region are reported in this paper. We then consider several astrophysical applications, including the possible influence interstellar PAHs may have on the NIR portion of the extinction curve and their role in pumping the IR emission features.

## 2. EXPERIMENTAL

The matrix isolation infrared spectroscopy techniques employed in these studies have been described in detail previously (Hudgins & Allamandola 1995a; Hudgins & Sandford 1998) and will be summarized here only briefly. Matrix-isolated PAH samples were prepared by vapor codeposition of the species of interest with an overabundance of argon onto a 14 K CsI window suspended in a high-vacuum chamber ( $p < 10^{-8}$  torr). The samples were vaporized from heated Pyrex tubes, while argon was admitted through an adjacent length of copper tubing cooled by liquid nitrogen,  $N_2(l)$ . Deposition temperatures for the individual PAHs are provided in Table 1. Estimates based on the characteristic band intensities of PAHs and the calibrated argon deposition rate place the Ar/PAH ratio in these experiments in excess of 1000/1 (Hudgins & Sandford 1998). The PAH samples used in this investigation were obtained from a variety of sources. PAHs 15–27 (see Table 1) were obtained from Professor Werner Schmidt, Institute for PAH Research, Germany. Sources for PAHs 1–14 are identified in Hudgins et al. (2000) and Hudgins & Allamandola (1997, 1995a, 1995b). Although some of the samples are of unspecified purity, the absence of any notable discrepant spectral features between the theoretical and experimental mid-infrared spectra indicates that impurity levels are no more than a few percent.

All NIR spectra reported here were measured at  $2\text{ cm}^{-1}$  resolution by co-adding 500 scans or more on either a Nicolet 740 or Digilab Excalibur 4000 Fourier transform infrared spectrometer. The spectra measured with the Nicolet 740 spanned the  $15000\text{--}9000\text{ cm}^{-1}$  ( $0.66\text{--}1.11\text{ }\mu\text{m}$ ) range, and those measured with the Excalibur 4000 covered the  $15000\text{--}4000\text{ cm}^{-1}$  ( $0.66\text{--}2.5\text{ }\mu\text{m}$ ) range. Mid-infrared spectra ( $4000\text{--}500\text{ cm}^{-1}$ ,  $2.5\text{--}20\text{ }\mu\text{m}$ ) were measured for each of these samples as well and are reported elsewhere (see mid-IR cross references in Table 1). The  $15000\text{--}9000\text{ cm}^{-1}$  ( $0.66\text{--}1.11\text{ }\mu\text{m}$ ) spectra were collected using an NIR source, a quartz beam splitter, and a silicon detector. PAH spectra between  $11000$  and  $7000\text{ cm}^{-1}$  ( $0.91\text{--}1.43\text{ }\mu\text{m}$ ) were collected using the spectrometer's NIR source (tungsten lamp) in conjunction with a quartz beam splitter and a liquid nitrogen-cooled MCT-B detector (typically used for the mid-IR). Spectra between  $7000$  and  $500\text{ cm}^{-1}$  ( $1.43$  and  $20\text{ }\mu\text{m}$ ) were collected using the MCT-B detector in combination with a KBr beam splitter. The number of scans was chosen to optimize both the signal-to-noise ratio as well as time requirements of each experiment. The spectra of PAHs numbered 1–14 in Table 1 and shown in Figures 1, 2, and 3 were measured using the Nicolet 740 as part of our initial mid-IR studies and do not include the  $9000\text{--}4000\text{ cm}^{-1}$  ( $1.11\text{--}2.5\text{ }\mu\text{m}$ ) region. These spectra were

measured in the configuration described earlier. The spectra of PAHs 4 and 7 were also measured out to  $7000\text{ cm}^{-1}$  using the Digilab spectrometer.

PAH ions were generated by in situ vacuum ultraviolet photolysis of the matrix-isolated neutral PAH compound. This was accomplished with the combined  $120\text{ nm Ly}\alpha$  ( $10.1\text{ eV}$ ) and the  $160\text{ nm}$  molecular hydrogen emission bands (centered around  $7.8\text{ eV}$ ) from a microwave-powered discharge in a flowing  $H_2$  gas mixture at a dynamic pressure of  $150\text{ mtorr}$ . Comparison of the pre- and postphotolysis mid-infrared spectra permits identification of PAH ion features (Hudgins et al. 2000) and allows for the determination of the percent ionization of the sample (Mattioda et al. 2003). Assuming that all neutral PAH molecules that disappear are converted into ions, we can derive an upper limit to the ionization efficiency by measuring the percent decrease in the integrated areas of the neutral mid-infrared bands that accompanies photolysis. Ionization efficiencies are typically around 15%, but vary based on PAH size and structure. To confirm the attribution of a photoproduct band, in both the mid- and near-infrared spectrum, to the PAH cation, parallel experiments were conducted in which the argon matrix was doped with an electron acceptor,  $NO_2$ , at a concentration of approximately 1 part in 1200. The presence of this electron acceptor quenches the formation of anions and enhances the production of cations.

Integrated intensities ( $\int \tau d\nu$ ) for individual bands were determined using the Win-IR Pro spectrometer control/data analysis software package provided by Digilab. Absolute intensities [ $A = (\int \tau d\nu)/N$ , where  $\tau$  is the optical depth and  $N$  is the density of absorbers in molecules  $\text{cm}^{-2}$ ] for the experimentally measured near-infrared bands were calculated as follows. The total number of absorbers (PAH molecules) was determined by taking the ratio of the sum of the experimental integrated band areas between  $1600$  and  $500\text{ cm}^{-1}$  ( $6.25$  and  $20\text{ }\mu\text{m}$ ) to the total theoretical sum for the same region,

$$N = \frac{\sum_{500}^{1600} A^{\text{exp}}}{\sum_{500}^{1600} A^{\text{thy}}}.$$

This range was chosen to exclude the contributions of (1) the far-infrared bands ( $\nu < 500\text{ cm}^{-1}$ ) that were not measured in the experiment; (2) the CH stretching bands, whose intensities are substantially overestimated by the calculations (Bauschlicher & Langhoff 1997; Hudgins & Sandford 1998); and (3) the overtone/composition bands in the  $2000\text{--}1650\text{ cm}^{-1}$  ( $5\text{--}6.1\text{ }\mu\text{m}$ ) region, whose intensities are not calculated in the theoretical results. This method takes advantage of the fact that although there may be significant band-to-band variability in the accuracy of the calculated intensity, the total intensity is generally accurate to 10%–20%, excluding the C–H stretching region. Based on the total surface density of absorbers ( $N$ ) and the upper ionization limit (determined by the percent decrease in the integrated areas of the neutral mid-infrared bands accompanying photolysis), one can calculate the number of ions present in each experiment and thus the  $A$ -values (in  $\text{km mol}^{-1}$ ) presented in Table 1 as well as Tables 2–12. Similarly, all spectra have been normalized to include the same number of ions ( $1 \times 10^{15}$ ).

For presentation purposes only, the data have been baseline corrected. The anion figures were obtained by subtracting off the cation bands (obtained from the Ar/ $NO_2$  matrix isolation experiment), using the Win-IR software package. No further

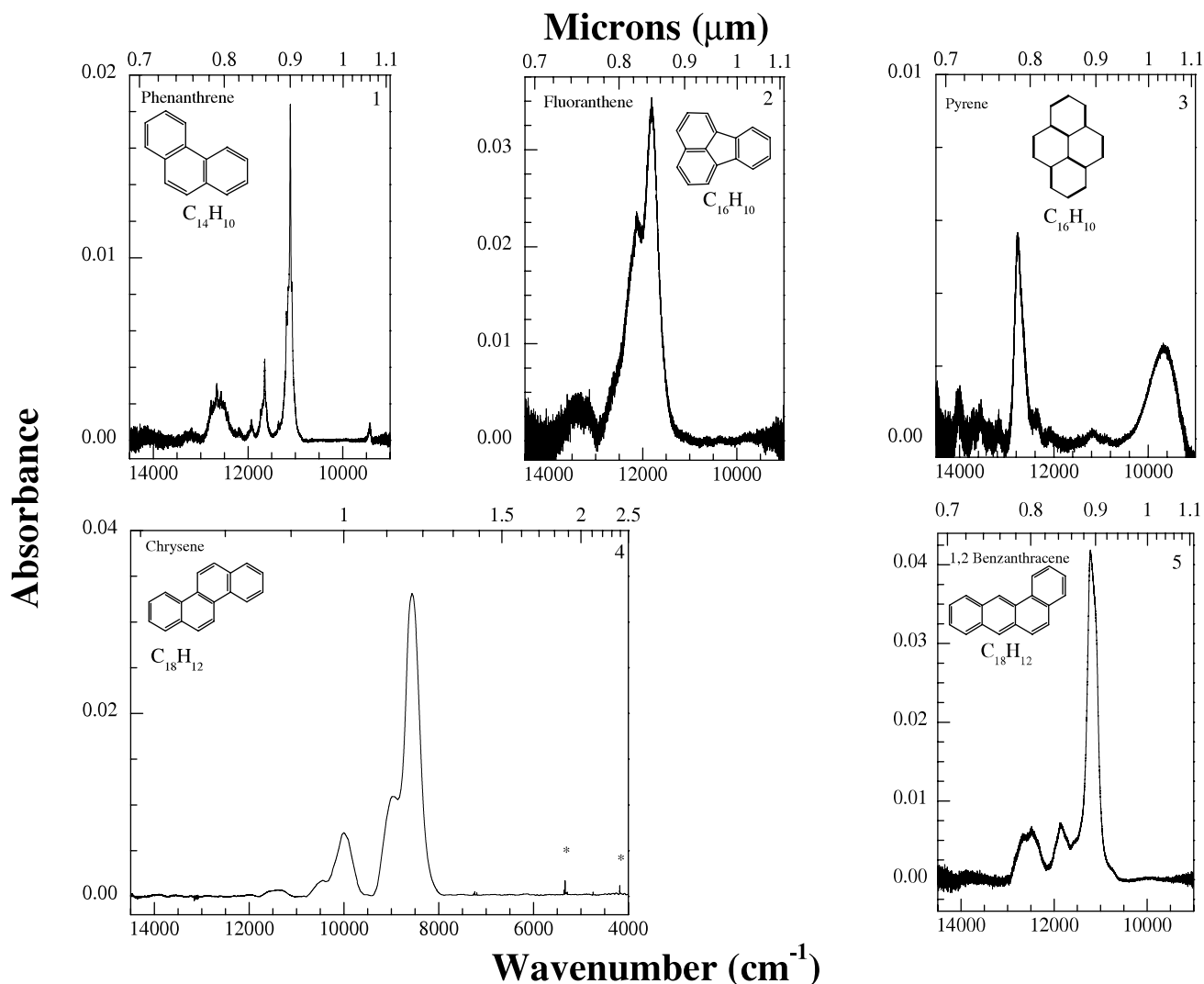


Fig. 1.—Matrix-isolated near-IR absorption spectra for phenanthrene, fluoranthene, pyrene, chrysene, and 1,2-benzanthracene cations. The numbers in the upper right-hand corners correspond to the PAH numbers in Table 1. Spectra have been normalized to an equivalent number of ions ( $1 \times 10^{15}$ ). Asterisks indicate bands due to artifacts.

data reduction was necessary. All numerical values were obtained from the original (unaltered) data.

### 3. RESULTS

The near-infrared spectra of 27 different PAHs, ranging in carbon number from  $C_{14}$  to  $C_{50}$ , are presented here. Table 1 presents the names, formulae, structures, deposition temperatures, total NIR band strengths, and cross references to other relevant spectroscopic studies. The PAHs are listed in order of increasing carbon number in the table with the numbers in the first column used as identifiers for each PAH throughout the text. The corresponding spectra are presented in Figures 1–6, with peak positions and integrated absorbance values for the major bands listed in Tables 2–12.

#### 3.1. Near-Infrared Spectral Characteristics

Inspection of Table 1 shows that the PAHs studied here can be divided into two groups, small PAHs ( $C_{14}H_{10}$  to  $C_{24}H_{12}$ ) and large PAHs ( $C_{34}H_{16}$  to  $C_{50}H_{22}$ ). In general, the spectra for the small PAHs (Figs. 1, 2, and 3) cover the range from 14000 to 9000  $cm^{-1}$  (0.7–1.1  $\mu m$ ), and the spectra for the large PAHs (Figs. 3, 4, 5, and 6) cover the 14000–4000  $cm^{-1}$  (0.7–2.5  $\mu m$ )

range. Spectra between 14000 and 4000  $cm^{-1}$  were also measured for the small PAHs 4 and 7. Although a feature was detected at 1.17  $\mu m$  (8560  $cm^{-1}$ ) in the extended molecule 4 spectrum, no additional features were identified in molecule 7. Since the purpose of this paper is to present a summary of the overall NIR spectroscopic properties of these species, rather than a detailed analysis of each spectrum, only general trends within each of these groups are described in this section. Detailed spectroscopic discussions for some of the PAH spectra presented here can be found in the electronic transition cross references listed in Table 1. Most spectra tend to be dominated by a single strong band or a cluster of strong bands falling between 13000 and 8000  $cm^{-1}$  (0.77 and 1.25  $\mu m$ ). While bands from the smaller species tend to fall at the upper end of this range, the larger species absorb at the lower end. Anion bands, when present, tend to be substantially weaker than those of the corresponding cation.

The 14 small PAH spectra presented in Figures 1–3 show that in the 14000–9000  $cm^{-1}$  (0.7–1.1  $\mu m$ ) region, many are dominated by a strong “narrow” band (full width at half-height [FWHH]  $< 500 cm^{-1}$ ) with clear vibronic substructure to the blue. Following Andrews et al. (1985) and assigning the

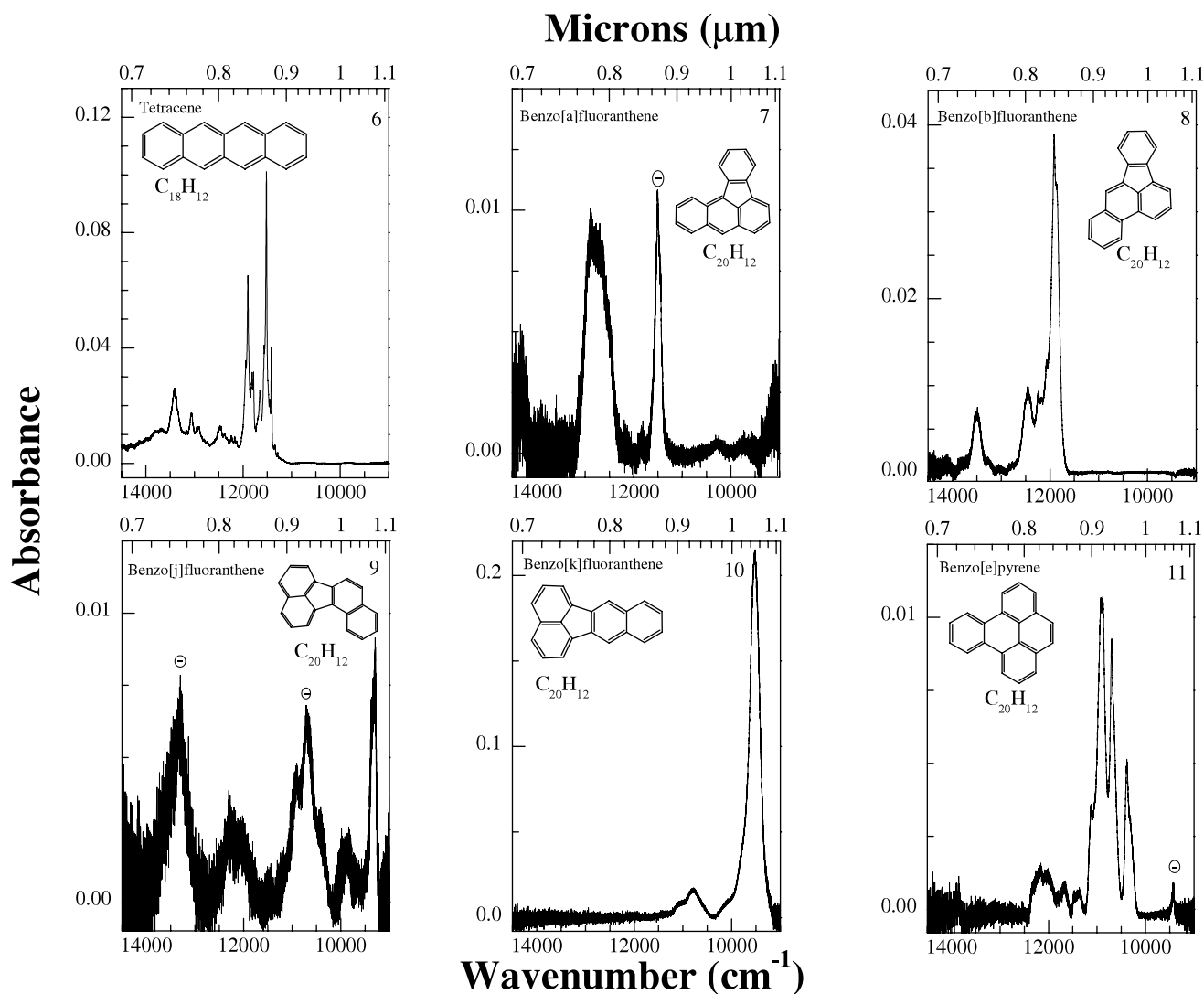


FIG. 2.—Matrix-isolated near-IR absorption spectra for tetracene, benzo[a]fluoranthene, benzo[b]fluoranthene, benzo[j]fluoranthene, benzo[k]fluoranthene, and benzo[e]pyrene cations. Anion features are indicated by a circled minus sign above the band. Spectra have been normalized to an equivalent number of ions ( $1 \times 10^{15}$ ). The numbers in the upper right-hand corners correspond to the PAH numbers in Table 1.

prominent absorption to the 0–0 band for PAHs 1, 4, 5, and 8, vibronic bands with spacings lying  $600\text{--}800\text{ cm}^{-1}$  and  $1200\text{--}1600\text{ cm}^{-1}$  to the blue are clearly present. For example, the spectrum of 1,2-benzanthracene (PAH 5) is dominated by the peak at  $0.8913\text{ }\mu\text{m}$  ( $11220\text{ cm}^{-1}$ , FWHH  $\sim 250\text{ cm}^{-1}$ ), with two clear bands to the blue centered near  $0.8434$  and  $0.8010\text{ }\mu\text{m}$  ( $11860$  and  $12490\text{ cm}^{-1}$ ). In this case, the spacings between the prominent band and the two satellite bands are  $640$  and  $1270\text{ cm}^{-1}$ , respectively. This vibronic band pattern is also evident for PAHs 6, 11, 13, and 14; however, for these species band splitting is severe. These vibronic spacings correspond to progressions involving the CH out-of-plane bends and CC stretching vibrations, respectively, and are similar to a pattern seen in the vibronic absorption spectra of many (not all) PAH cations (e.g., Andrews et al. 1985; Salama & Allamandola 1991). In addition, several of the small PAH spectra show very broad (FWHH  $> 500\text{ cm}^{-1}$ ), prominent features (PAHs 2, 7, and 9). Interestingly, of the five PAHs containing a pentagonal ring, three of them (PAHs 2, 7, and 9) have exceptionally broad, strong absorption bands. Finally, of these 14 small PAHs, only three show bands that can be exclusively attributed to the anion, PAHs 7, 9, and 11. Two of these incorporate a pentagonal ring.

The 13 larger PAH spectra shown in Figures 3–6 cover the range from  $14000$  to  $4000\text{ cm}^{-1}$  ( $0.7\text{--}2.5\text{ }\mu\text{m}$ ). As with the smaller PAH spectra, some have prominent broad features (PAHs 21, 24, 25, and 27), and a few are dominated by a narrow band with weak satellite bands indicating a vibronic progression involving the CH out-of-plane bending and CC stretching modes (PAHs 16, 17, and 18). The spectra of PAHs 19 and 23 may also show this pattern; however, band splitting or broadening is severe for these molecules. Of particular interest for these larger PAHs is the higher fraction for which bands solely attributable to the anion form appear (PAHs 15, 16, 17, 18, 19, 20, 21, 24, 25, 26, and 27). This is consistent with PAH electron affinity increasing with size.

Where appropriate, Table 1 includes cross references to other experimental and theoretical studies of the electronic transitions in isolated PAHs. Andrews and collaborators measured the first optical spectra of several PAH cations isolated in an argon matrix (Andrews & Blankenship 1981; Andrews et al. 1985). This work included PAHs 1, 4, 5, and 6 studied here. There is excellent agreement in band positions, profiles, and relative intensities for the common wavelength regions considered in these two studies. The NIR electronic spectrum of the phenanthrene (PAH 1) cation has also been studied in a neon matrix (Salama

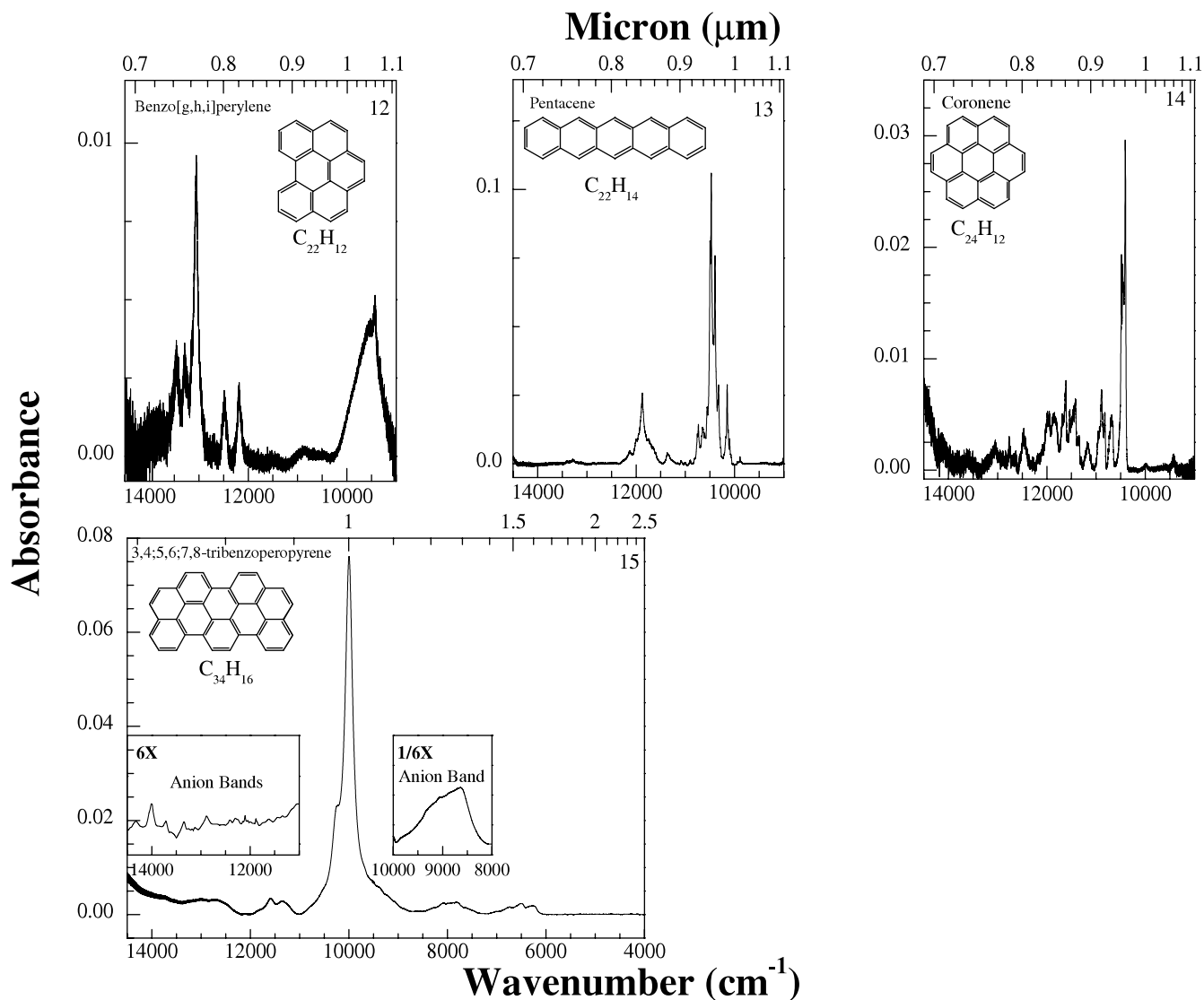


Fig. 3.—Matrix-isolated near-IR absorption spectra for benzo[*g,h,i*]perylene, pentacene, coronene, and 3,4;5,6;7,8-tribenzoperopyrene cations. Anion bands are displayed as insets. Spectra have been normalized to an equivalent number of ions ( $1 \times 10^{15}$ ). The numbers in the upper right-hand corners correspond to the PAH numbers in Table 1.

et al. 1994) and the gas phase (Bréchnac & Pino 1999). The general features of the spectrum shown in Figure 1, a strong, narrow feature near  $11000 \text{ cm}^{-1}$  ( $0.9 \mu\text{m}$ ) with two moderately strong and two weak vibronic bands to the blue, repeat in all cases. Both the neon and argon matrix bands are redshifted with respect to the gas-phase lines by roughly  $100 \text{ cm}^{-1}$ , with the peaks in an argon matrix about  $25 \text{ cm}^{-1}$  to the red of those in a neon matrix. The gas-phase phenanthrene cation absorption lines are much narrower than the matrix bands. Interestingly, the FWHHs for the phenanthrene cation bands, when phenanthrene is isolated in an argon matrix (FWHH =  $60 \text{ cm}^{-1}$ ), are significantly smaller than those measured for the phenanthrene cation isolated in a neon matrix (FWHH =  $700 \text{ cm}^{-1}$ ). The electronic spectrum of PAH 25, isolated as a cation in a neon matrix, has also been reported (Ruiterkamp et al. 2002). As above, the argon and neon matrix spectra are very similar. Although there is a much larger redshift, about  $220 \text{ cm}^{-1}$ , between the main peak positions in neon and argon, the FWHH is significantly smaller in an argon matrix ( $440 \text{ cm}^{-1}$ ) than in a neon matrix ( $930 \text{ cm}^{-1}$ ). The electronic spectrum of the pyrene cation (PAH 3) isolated in an argon matrix from 200 to 800 nm ( $50000\text{--}12500 \text{ cm}^{-1}$ ) has been ana-

lyzed by Vala et al. (1994). There is excellent agreement between the pyrene cation spectrum discussed here and that reported by Vala et al. in the wavelength region common to both studies.

The theoretically determined vertical excitation energies (in eV) have been compared with tabulated experimental values for nine of the 14 small PAH ions listed in Table 1 (Hirata et al. 2003). Although Hirata et al. do not present the spectra from which the experimental vertical energies were determined, in the regions of overlap, there is very good agreement between their listed experimental values in eV and the positions of the bands in Figures 1–3.

### 3.2. Near-Infrared Band Intensities

Given the astrophysical importance of quantitative band strengths as well as spectral band information, integrated absorbance values ( $\text{km mol}^{-1}$ ) for the bands in the spectra shown in Figures 1–6 are listed in Tables 2–12. While it is not customary to describe band strengths of electronic transitions in units of  $\text{km mol}^{-1}$ , we do so here in order to facilitate comparisons with mid-IR band strengths, which are normally presented in these units. These data are also presented as oscillator

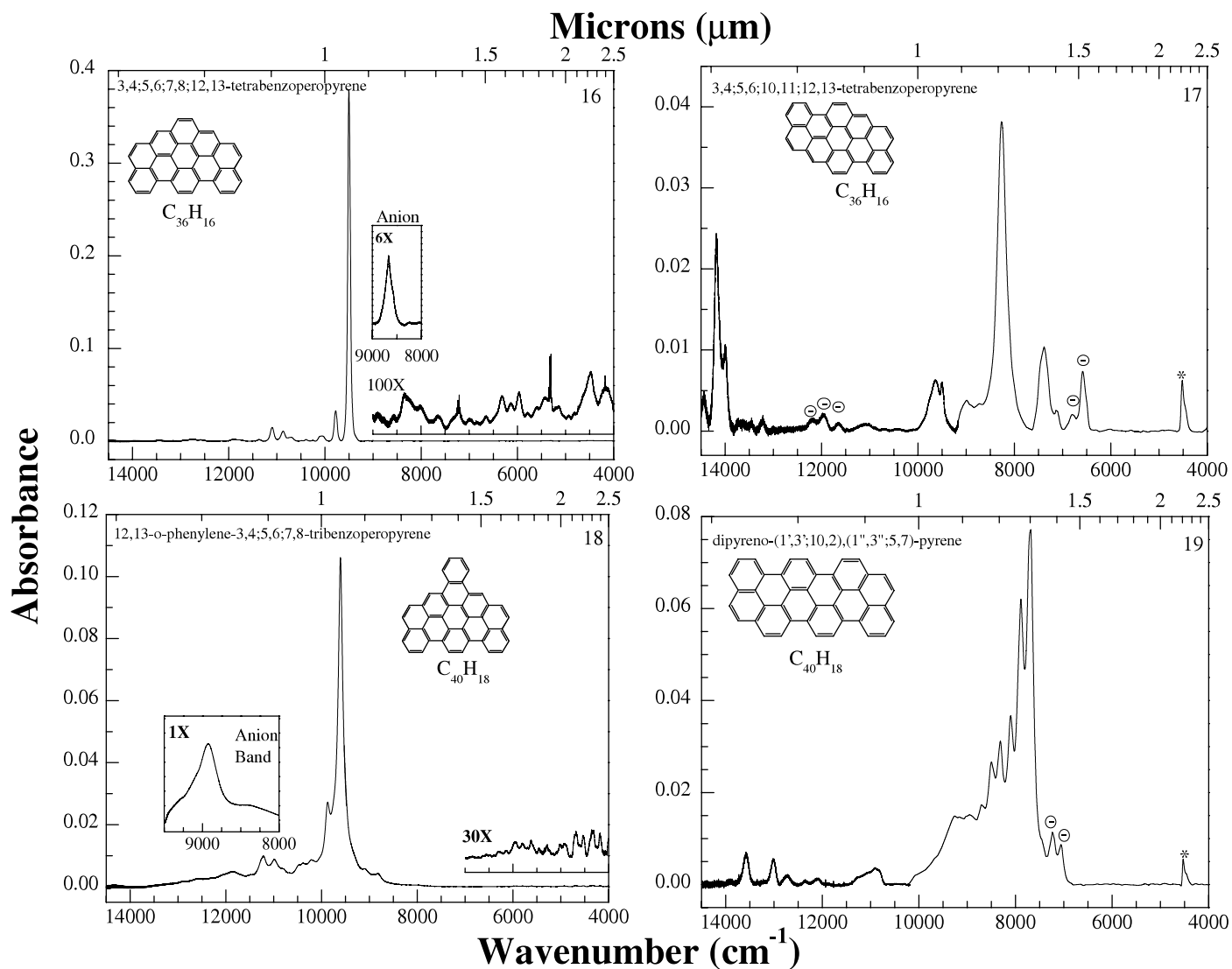


FIG. 4.—Matrix-isolated near-IR absorption spectra for 3,4;5,6;7,8;12,13-tetrabenzoperopyrene, 3,4;5,6;10,11;12,13-tetrabenzoperopyrene, 12,13-*o*-phenylene-3,4;5,6;7,8-tribenzoperopyrene, and dipyreno-(1',3';10,2),(1'',3'';5,7)-pyrene cations. Anion features are displayed as insets or are indicated by a circled minus sign above the band. Spectra have been normalized to an equivalent number of ions ( $1 \times 10^{15}$ ). The numbers in the upper right-hand corners correspond to the PAH numbers in Table 1.

strength,  $f$ , in Table 1 as well as in Tables 2–12. For Table 1, the oscillator strength is defined over all of the bands that make up an electronic transition, not individual vibronic components; the integrated absorbance values ( $\text{km mol}^{-1}$ ) for each of the bands in an individual spectrum were summed before the conversion to  $f$  was made. Thus, the oscillator strength reported in Table 1 is derived from the total integrated area of the bands shown in Figures 1–6. The oscillator strength was determined by multiplying the total integrated absorbance by  $1.87 \times 10^{-7} \text{ mol km}^{-1}$  (Kjaergaard et al. 2000). Implicit in this conversion is the assumption that most of the strength of the bands corresponding to the electronic transition appears in the spectral regions studied. While this may not be the case for some of the PAHs, especially 1–14, it probably holds for most. Table 1 lists both oscillator strength and total integrated absorbance values in units of  $\text{km mol}^{-1}$ . The reliability of these  $f$ -values is discussed further below.

For most of the small PAHs considered here (PAHs 1–14, Table 1), the oscillator strengths range from  $3 \times 10^{-3}$  up to  $3 \times 10^{-2}$ . Within this size range the benzo[*k*]fluoranthene cation

(PAH 10) stands out with  $f = 8 \times 10^{-2}$ . As one would anticipate, the oscillator strengths for most of the larger PAHs (15–27) are slightly larger, falling between  $1.9 \times 10^{-2}$  and  $6.3 \times 10^{-2}$ . However, there are two remarkable exceptions in the sample considered here, PAHs 25 and 27, with oscillator strengths of  $2.6 \times 10^{-1}$  and  $1.3 \times 10^{-1}$ , respectively. We have considered possible connections between  $f$ -values and parameters such as molecular size (as measured in carbon number), structure, and C/H ratio. Apart from a loose correlation of  $f$  with carbon number, none of these other molecular properties strongly influences  $f$  behavior, as one might expect given such a diverse population of PAH molecular structures.

Theoretically calculated oscillator strengths are available for nine of the small PAHs considered here, and they are also presented in Table 1. The theoretical values are larger than the experimental values, and the variance is quite large. For most of these species,  $f_{\text{th}}/f_{\text{exp}}$  lies between about 1.3 and 10. The largest discrepancy, 30, is associated with phenanthrene (PAH 1), the smallest PAH considered here. In spite of its fundamental astrophysical importance, determining reliable PAH ion oscillator

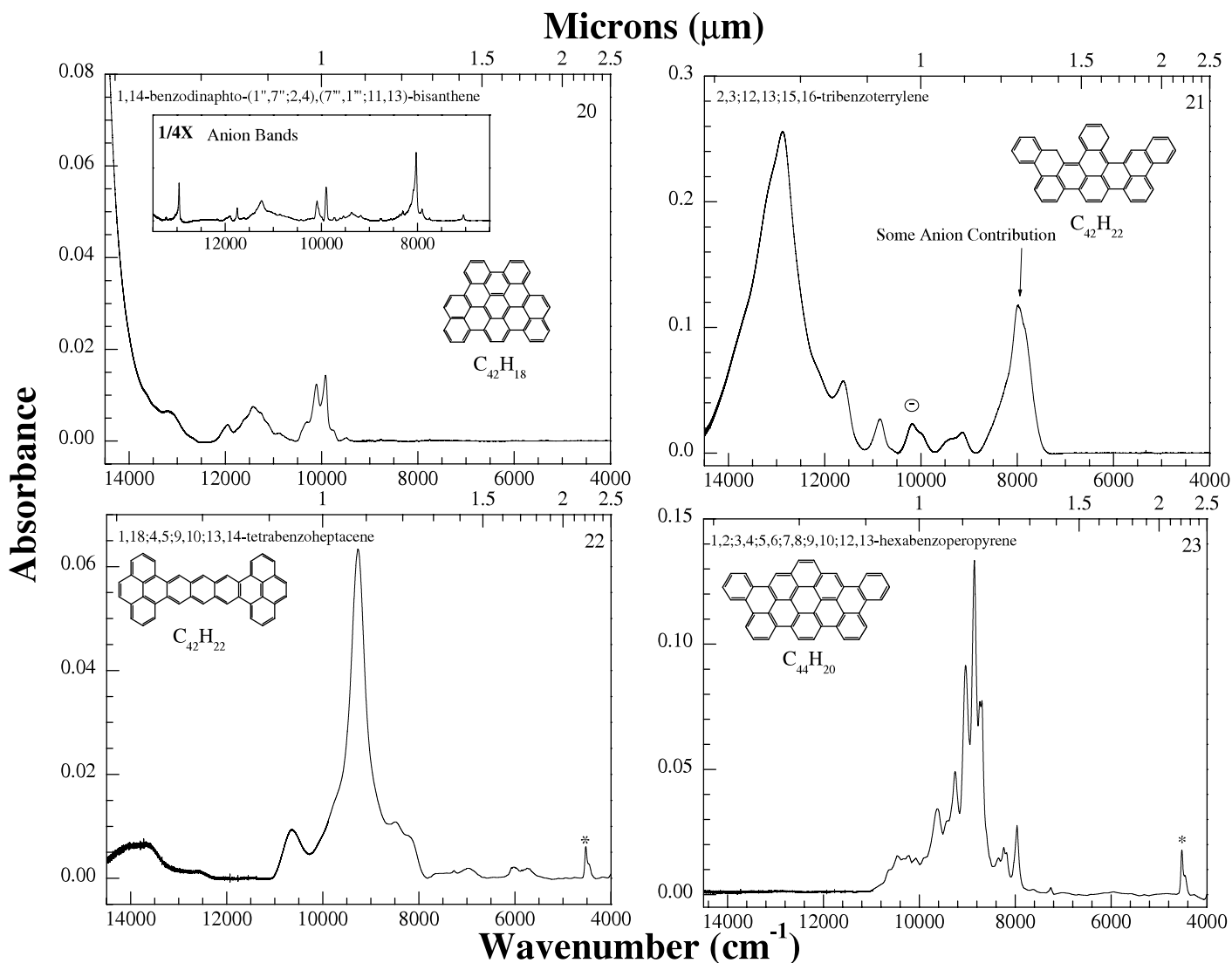


FIG. 5.—Matrix-isolated near-IR absorption spectra for 1,14-benzodipnaphtho-(1',7'';2,4),(7''',1''';11,13)-bisanthene, 2,3;12,13;15,16-tribenzoterrylene, 1,18;4,5;9,10;13,14-tetrabenzoheptacene, and 1,2;3,4;5,6;7,8;9,10;12,13-hexabenzoperopyrene cations. Anion features are displayed as insets or are indicated by a circled minus sign above the band. Spectra have been normalized to an equivalent number of ions ( $1 \times 10^{15}$ ). The numbers in the upper right-hand corners correspond to the PAH numbers in Table 1.

strengths for electronic transitions experimentally has proven particularly challenging (Hudgins & Allamandola 1995b; Salama & Allamandola 1991). Due to the inherent difficulty in maintaining a stable, isolated PAH ion population, the vast majority of spectroscopic studies have been carried out in inert gas matrices. Comparisons between gas-phase and matrix isolation spectroscopic studies with quantum calculations have shown that matrix perturbations are minor when studying PAH ion *vibrational* transitions, which give rise to the well-known interstellar infrared emission bands (e.g., Hudgins & Allamandola 2004; Mattioda et al. 2003), and matrix isolation studies can be directly applied to the interstellar IR emission bands. This is *not* generally so for electronic transitions, which give rise to bands spanning the UV to the NIR spectral range. As illustrated above by the NIR band shifts and FWHM variations between argon and neon matrices and gas-phase studies, the matrix environment can severely perturb intrinsic *electronic* band positions and band shapes. Thus, it is possible that electronic transition band strengths are perturbed as well. The matrix influence on band strengths is not only matrix dependent, but is also influenced by other species present (Hudgins &

Allamandola 1995a). Furthermore, it also appears to depend on the method of determination. For example, Salama et al. (1994) studied the electronic transition of the neon matrix-isolated phenanthrene cation corresponding to the same transition reported here for phenanthrene (PAH 1) in an argon matrix. Salama et al. calculated the number of phenanthrene ions produced from the reduction in the absorbance of the neutral phenanthrene *electronic* bands in the UV. This is in contrast to the method employed here in which the number of phenanthrene ions produced is determined by the reduction in the absorbance of the neutral phenanthrene *vibrational* bands in the mid-IR. The discrepancy is unacceptably large. Salama et al. report an  $f$ -value of  $6 \times 10^{-5}$  for this phenanthrene cation transition in a neon matrix, while we determine  $f = 3.5 \times 10^{-3}$  from the argon matrix data. These values are to be compared with theoretical values that range from 0.096 to 0.16. To the best of our knowledge, the pyrene cation (PAH 3) is the only other PAH cation for which theoretical and experimental NIR oscillator strengths have been reported. In contrast to the theoretical value of 0.015 (Hirata et al. 2003), Vala et al. (1994) report  $f \sim 0.008$ , compared to our value of  $f \sim 0.004$ . Ehrenfreund

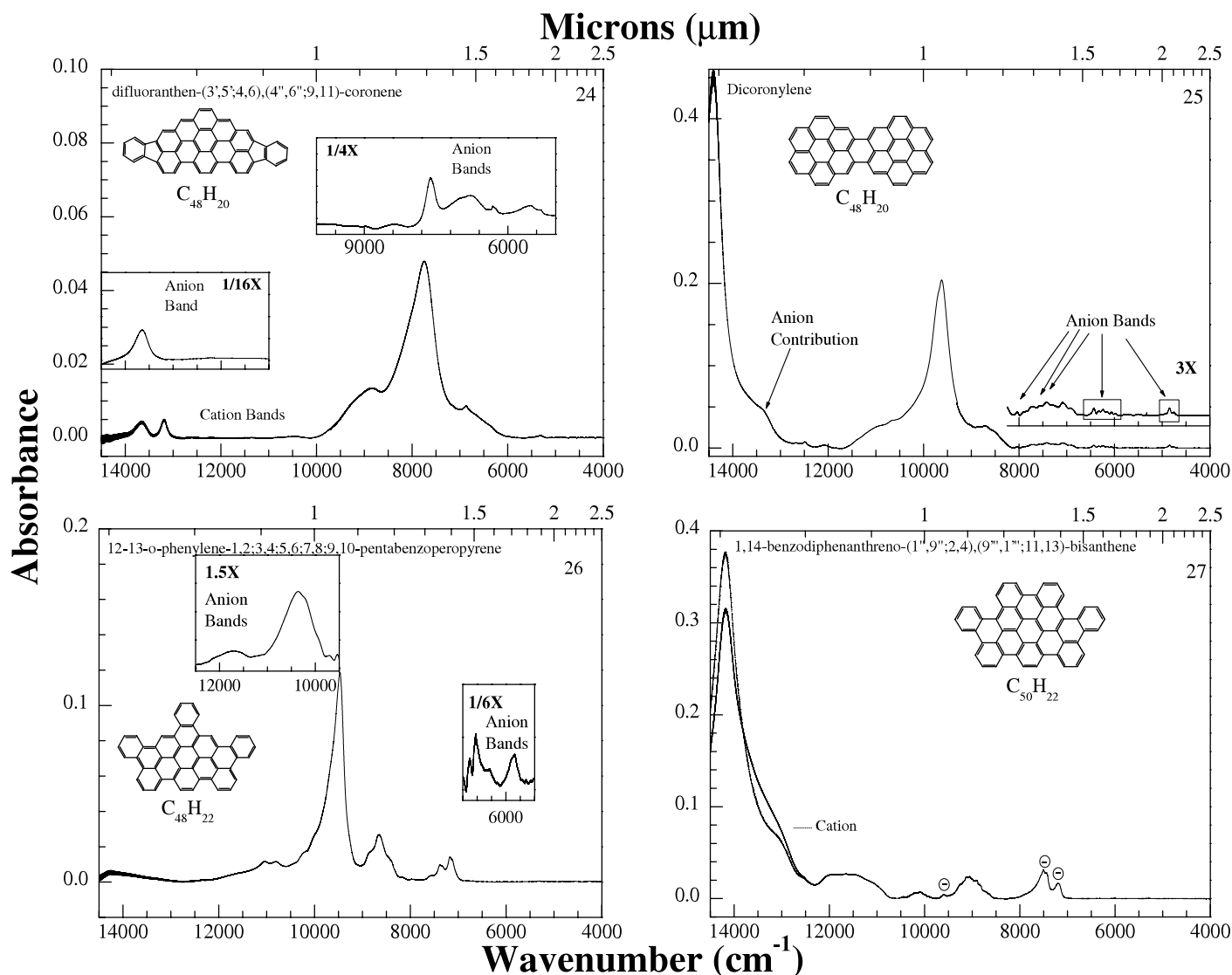


FIG. 6.—Matrix-isolated near-IR absorption spectra for difluoranthren-(3',5';4,6),(4'',6'';9,11)-coronene, dicoronylene, 12,13-*o*-phenylene-1,2;3,4;5,6;7,8;9,10-pentabenzoperopyrene, and 1,14-benzodiphenanthreno-(1'',9'';2,4),(9''',1''';11,13)-bisanthene cations. Anion features are displayed as inserts or are indicated by a circled minus sign above the band. Spectra have been normalized to an equivalent number of ions ( $1 \times 10^{15}$ ). The numbers in the upper right-hand corners correspond to the PAH numbers in Table 1.

et al. (1995) have measured the NIR spectrum for the coronene cation isolated in an argon matrix and determined  $f \sim 0.005$ . This compares favorably with our value of  $f \sim 0.006$ . In summary, there is a large variation in reported PAH ion oscillator strengths, regardless of the means of determination. In those cases for which argon matrix data are available, differences of at most a factor of 2 are encountered. Inspection of Table 1 shows that when theoretical data are available, most of our experimental values are 1.3–10 times smaller. Given that the  $f$ -values listed in Table 1 represent the largest collection of experimentally determined PAH ion oscillator strengths, we use these below.

#### 4. ASTROPHYSICAL CONSIDERATIONS

The spectra shown in Figures 1–6 and corresponding absolute absorption strengths listed in Tables 2–12 illustrate that PAH ions have NIR transitions that warrant consideration when evaluating the effects of PAHs on the interstellar radiation field. Here we consider two applications that impact observations: the ability of NIR photons to pump the mid-IR PAH emission

bands, and the possibility that PAHs can impose broadband structure on the interstellar extinction curve in addition to contributing to the discrete DIBs.

##### 4.1. Pumping the Mid-IR PAH Emission Features with NIR Photons

An important and long-standing issue concerning the model that IR fluorescence from highly vibrationally excited PAHs is responsible for the interstellar mid-IR emission features has to do with the excitation mechanism. While several processes such as chemical and electron-ion recombination reactions and radiative pumping can produce highly vibrationally excited species, the early association of the interstellar emission bands with UV-rich sources pointed to radiative excitation as the principal excitation mechanism of the unidentified infrared (UIR) features (Allamandola et al. 1979). With time, pumping by UV radiation became a central tenet of all PAH models because of this association of the interstellar emission bands with UV-rich sources and because PAHs have strong, broad UV absorption bands (Allamandola et al. 1989; Puget & Leger 1989; Schutte



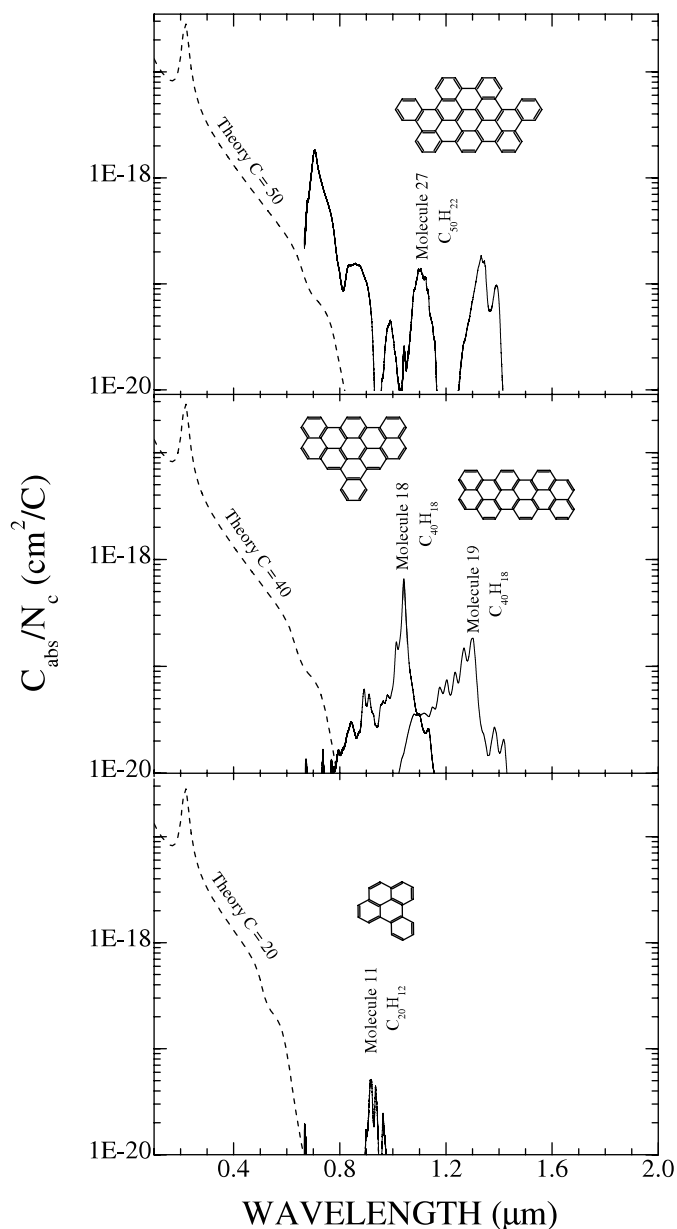


FIG. 7.—NIR absorption cross section (per C atom) of PAHs containing  $N_C = 20, 40,$  and  $50$  C atoms taken from the spectra presented in § 3 compared with the theoretical absorption cross section of like-sized PAHs determined using the formalism described in Li & Draine (2001) for generic astronomical PAH molecules.

et al. 1993; Pech et al. 2002; Verstraete et al. 2001). However, if radiative pumping was the excitation mechanism, early work by Aitken & Roche (1983) already indicated that, to avoid UV to IR photon fluorescent efficiencies exceeding unity, excitation by visible photons would be required to account for the mid-IR band intensities from NGC 7027. More recently, this tenet of the PAH model has been questioned by very careful observations of the mid-IR emission from a number of UV-poor reflection nebulae by Uchida et al. (1998, 2000), which show that the UIR spectrum is present and largely independent of stellar type for B- to F-type stars.

While small neutral PAHs have a steep and sharp absorption cutoff in the UV with weaker absorption extending into the visible, this cutoff smoothly moves to longer wavelength with increasing PAH size (Birks 1970). Since this absorption characteristic of neutral (closed shell) species was incorporated in

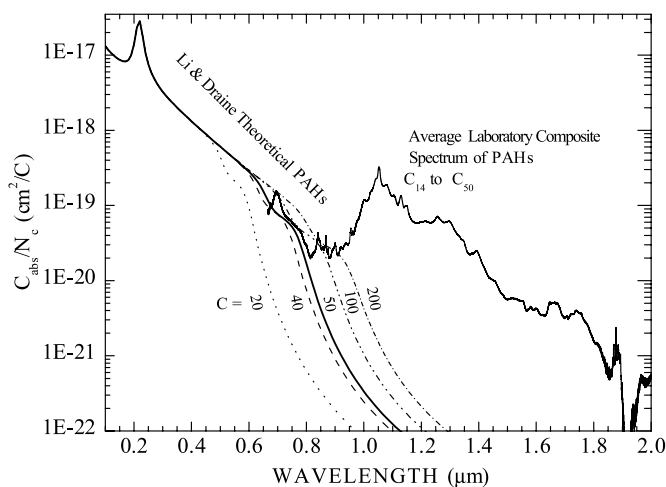


FIG. 8.—Average wavelength-dependent experimental NIR cross sections produced by the PAHs listed in Table 1 ( $N_C = 14\text{--}50$ ) compared with the modeled cross sections for PAHs with  $N_C = 20, 40, 50, 100,$  and  $200$  C atoms.

most PAH emission models (Schutte et al. 1993; Li & Draine 2001; Bakes et al. 2001), these models could not account for observations of the UIR bands from UV-poor objects. However, as shown here in detail, upon ionization the neutral PAH electronic configuration changes from closed shell to open shell (radical), and moderate to strong transitions at considerably longer wavelengths become possible (see references listed in Table 1 and Salama et al. [1996] and references therein for discussions of the theory). Extending their model to include this size and charge dependence, Li & Draine (2002) showed that PAHs could account for the UIR emission features in these UV-poor reflection nebulae. However, since the number of visible and near-IR PAH ion experimental spectra available upon which to extend their model was limited, they extrapolated the cutoff wavelength in accord with the data then available.

The predicted wavelength-dependent absorption cross sections derived using the formalism developed in Li & Draine (2002) for specific-sized PAHs are compared with the measured wavelength-dependent NIR absorption cross sections of four individual PAHs in Figure 7. The experimental cross sections for all of the PAHs listed in Table 1 were determined from the NIR absorption spectra presented in § 3. This comparison shows that ionized PAHs absorb with substantial strength at significantly longer wavelengths than predicted for the modeled generic “astronomical PAHs.” Figure 8 extends this by comparing the wavelength-dependent theoretical absorption cross sections of substantially larger astronomical PAHs to the wavelength-dependent NIR cross section produced by co-adding the experimental cross sections for all the PAHs listed in Table 1 and dividing by the total number of PAHs in the sample. Remarkably, this comparison shows that although they only span the size range from  $C_{14}$  through  $C_{50}$ , these ionized PAHs absorb with substantial strength at significantly longer wavelengths than predicted even for large, several-hundred-C-atom-sized PAHs.

These data show that radical PAH ions readily absorb near-IR photons, permitting the pumping of PAHs into highly vibrationally excited states, which then relax via emission of IR photons even in UV-poor regions. In a separate publication we develop a semiempirical model that takes these new NIR data into account, and we assess the relative importance of NIR and UV-visible photons in pumping the mid-IR PAH emission features (Mattioda et al. 2005).

#### 4.2. Interstellar PAHs and the Extinction Curve

There is overwhelming evidence that ionized PAHs are widespread throughout the diffuse interstellar medium (Mattila et al. 1996; Onaka et al. 1996). NIR transitions in these species could impose detectable structure on the extinction curve. Here we estimate the extent of this possible contribution. The cases we consider are somewhat contrived, as there are likely many hundreds if not hundreds of thousands of different PAH molecular structures that could contribute spectroscopic structure to the extinction curve. Knowing neither the different structures nor their corresponding spectra, we approximate the situation as follows. Using the standard relationship,  $N_{\text{H}}/E(B - V) = 5.8 \times 10^{21}$  atoms  $\text{cm}^{-2}$  mag $^{-1}$  (Bohlin et al. 1978), where  $N_{\text{H}}$  is the number of hydrogen atoms per  $\text{cm}^2$  along the line of sight and  $E(B - V)$  is the reddening expressed in magnitudes taking  $3 \times 10^{-4}$  for the cosmic C/H ratio, the number of carbon atoms per  $\text{cm}^2$  per  $E(B - V)$  becomes  $N_{\text{C}}/E(B - V) = 1.7 \times 10^{18}$ . Assuming that 10% of the available cosmic carbon is in the form of free PAHs (e.g., Allamandola et al. 1989; Puget & Leger 1989), the number of C atoms tied up in free PAHs per  $\text{cm}^2$  per  $E(B - V)$  is then  $N_{\text{C-PAH}}/E(B - V) = 1.7 \times 10^{17}$ . This is, however, a very conservative lower limit for the total amount of cosmic carbon tied up in PAH structures, since the 10% value for the amount of available carbon in PAHs holds for those contributing to the mid-IR emission features. Larger PAHs, PAH clusters, and amorphous carbon particles rich in PAH structures that do not contribute to the mid-IR features must also be present, and many of these will also have NIR transitions. However, for the sake of this analysis we assume an average of 50 C atoms per PAH. In this case,  $N_{\text{PAH}} = 3.4 \times 10^{15} E(B - V)$  molecules  $\text{cm}^{-2}$ .

Assuming a situation in which 10% of the PAHs in the total PAH ion population all absorb at nearly the same wavelength, the optical depth ( $\tau = \ln I_0/I$ ) of a band in the NIR portion of the extinction curve produced by these PAHs is estimated as follows. The spectra and integrated absorbance values presented in § 3 show that PAH cations containing between 40 and 50 C atoms often possess a discrete absorption band near  $9000 \text{ cm}^{-1}$  ( $1.1 \mu\text{m}$ ) with a FWHH  $\sim 400 \text{ cm}^{-1}$  ( $\sim 0.04 \mu\text{m}$ ), having integrated absorbance values ( $A$ ) between roughly  $1.6 \times 10^5$  and  $6.9 \times 10^5 \text{ km mol}^{-1}$  ( $2.56 \times 10^{-14}$  and  $1.1 \times 10^{-13} \text{ cm molecule}^{-1}$ ). Since  $N_{\text{PAH}}A \approx (\tau) d\nu$ , the optical depth becomes  $N_{\text{PAH}}A/d\nu$ . Taking  $A \approx 5 \times 10^{-14} \text{ cm molecule}^{-1}$ ,  $d\nu = 400 \text{ cm}^{-1}$ , and  $N_{\text{PAH}} = 3.4 \times 10^{15} E(B - V)$  molecules  $\text{cm}^{-2}$  (for 10% of the PAH ion population) yields a  $\tau/\text{mag} = 0.04$  for an absorption band produced by these interstellar PAH molecules.

Thus, the data presented here suggest that there should be weak, but detectable, broadband structure originating in ionized PAHs superposed on the NIR portion of the interstellar extinction curve.

#### 5. CONCLUSIONS

The near-infrared (NIR) spectra and band strengths of a wide variety of polycyclic aromatic hydrocarbon (PAH) ions have been reported. Oscillator strengths and integrated absorbance values have been determined for these NIR transitions.

Many of the NIR spectra of the small PAH cations are dominated by a strong, narrow band and show clear weaker vibronic substructure to the blue due to progressions involving the CH out-of-plane bends and CC stretching vibrations. As with the smaller PAH spectra, some of the larger PAH cations have spectra with prominent broad features, while others are dominated by a narrow band with weak satellite bands indicating a vibronic progression involving the CH out-of-plane bending and CC stretching modes. While all the spectra show PAH cation bands, strong PAH anion features become more important in the spectra of the larger species.

Two astrophysical applications have been considered in the text. The first has to do with interstellar extinction. Since the spectra of ionized PAHs show strong NIR transitions, and PAHs are present in the interstellar medium, they could add detectable structure to the extinction curve. The band strengths reported here suggest that ionized interstellar PAHs should add weak, broadband structure to the NIR portion of the interstellar extinction curve. The second issue has to do with the important question, can UV-poor radiation fields pump the PAH bands? The data presented here show that open-shell PAH ions have significant absorption features in the near-infrared, and PAHs can be pumped into vibrationally excited states even in UV-poor regions.

It is also important to keep in mind that some structures of neutral PAHs can also have open-shell, radical electronic configurations, as do the ions studied here (e.g., Hudgins et al. 2001, 2005; Szczepanski et al. 2002), and these will also possess longer wavelength electronic transitions, albeit likely having lower cross sections than ionized open-shell species. Thus, even in regions dominated by nonionizing radiation, it may be possible to detect the emission or absorption from neutral, open-shell PAH species.

The research presented here was supported through the Long Term Space Astrophysics Program (399-20-40) with earlier support from NASA's Laboratory Astrophysics Program. Andrew Mattioda acknowledges the support of the National Research Council. We are deeply indebted to Robert Walker for his outstanding technical support of all phases of the experimental work. We also gratefully acknowledge very insightful discussions with Jan Cami concerning the impact of the NIR transitions on the extinction curve.


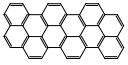


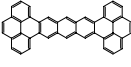





#### APPENDIX

Table 1 lists the PAHs used in this laboratory investigation, along with their designated number (for use with the figures), molecular formula, deposition temperature, total oscillator strength in the NIR, and appropriate references. Oscillator strengths for the individual PAH cation bands can be found in Tables 2–7, while the oscillator strengths of the individual PAH anion bands can be found in Tables 8–12. Tables 2–12 are arranged in order of increasing PAH size, in accordance with Table 1 and Figures 1–6.

TABLE 1  
NAME, FORMULA, STRUCTURE, AND RELATED INFORMATION FOR THE PAHS INVESTIGATED HERE

NUMBER	COMPOUND NAME	MOLECULAR FORMULA	CHEMICAL STRUCTURE	DEPOSITION TEMPERATURE (°C)	TOTAL $A$ Cation (Anion) ( $10^3 \text{ km mol}^{-1}$ )	OSCILLATOR STRENGTH $f$		REFERENCES		
						Cation (Anion) ( $10^{-3}$ )	Theory <sup>a</sup> ( $10^{-3}$ )	Mid-IR	NIR	
									Experimental	Theory
1.....	Phenanthrene	C <sub>14</sub> H <sub>10</sub>		10	19.0	3.5	96.0	1	1, 2, 3, 4	5
2.....	Fluoranthene	C <sub>16</sub> H <sub>10</sub>		45	140.0	26.0	71.0	6	...	5
3.....	Pyrene	C <sub>16</sub> H <sub>10</sub>		65	20.1	3.8	15.0	1, 7, 8	1, 7	5, 7, 9
4.....	Chrysene	C <sub>18</sub> H <sub>12</sub>		95	160.0	31.0	...	10	2	5
5.....	1,2-benz[ <i>a</i> ]anthracene	C <sub>18</sub> H <sub>12</sub>		85	120.0	22.0	67.0	10	2	5
6.....	Tetracene	C <sub>18</sub> H <sub>12</sub>		125	130.0	24.0	133	11, 13	2, 11, 13	5
7.....	Benzo[ <i>a</i> ]fluoranthene	C <sub>20</sub> H <sub>12</sub>		95	75.0 <sup>b</sup> (25.0)	14.0 (4.7)	...	6	...	...
8.....	Benzo[ <i>b</i> ]fluoranthene	C <sub>20</sub> H <sub>12</sub>		95	79.0	15.0	...	6	...	...
9.....	Benzo[ <i>j</i> ]fluoranthene	C <sub>20</sub> H <sub>12</sub>		95	40.0 (31.0)	7.5 (5.9)	...	6	...	...
10.....	Benzo[ <i>k</i> ]fluoranthene	C <sub>20</sub> H <sub>12</sub>		110	450.0	85.0	...	6	...	...
11.....	Benzo[ <i>e</i> ]pyrene	C <sub>20</sub> H <sub>12</sub>		105	25.0 (4.03)	4.7 (0.76)	6.0	1	1	5
12.....	Benzo[ <i>g,h,i</i> ]perylene	C <sub>22</sub> H <sub>12</sub>		130	31.0	5.9	57.0	1	1	5
13.....	Pentacene	C <sub>22</sub> H <sub>14</sub>		200	130.0	24.0	185.0	11, 12	11, 12, 14	5
14.....	Coronene	C <sub>24</sub> H <sub>12</sub>		155	32.0	6.1	8.0	1, 8	1, 15	5
15.....	3,4;5,6;7,8-tribenzo peropyrene	C <sub>34</sub> H <sub>16</sub>		314	180.0 (130.0)	34.0 (24.0)	...	16	...	...
16.....	3,4;5,6;7,8;12,13-tetrabenzo peropyrene	C <sub>36</sub> H <sub>16</sub>		325	220.0 (19.0)	40.0 (3.6)	...	16	...	...
17.....	3,4;5,6;10,11;12,13-tetrabenzo peropyrene	C <sub>36</sub> H <sub>16</sub>		335	110.0 (45.0)	21.0 (8.4)	...	16	...	...

TABLE 1—Continued

NUMBER	COMPOUND NAME	MOLECULAR FORMULA	CHEMICAL STRUCTURE	DEPOSITION TEMPERATURE (°C)	TOTAL <i>A</i>		OSCILLATOR STRENGTH <i>f</i>		REFERENCES		
					Cation (Anion) (10 <sup>3</sup> km mol <sup>-1</sup> )	Cation (Anion) (10 <sup>-3</sup> )	Theory <sup>a</sup> (10 <sup>-3</sup> )	Mid-IR	NIR		
									Experimental	Theory	
18.....	12,13- <i>o</i> -phenylene-3,4;5,6;7,8-tribenzoterrylene	C <sub>40</sub> H <sub>18</sub>		364	160.0 (62.0)	30.0 (12.0)	...	16	...	...	
19.....	Dipyreno-(1',3';10,2), (1'',3'',5,7)-pyrene	C <sub>40</sub> H <sub>18</sub>		396	170.0 (63.0)	32.0 (12.0)	...	16	...	...	
20.....	1,14-benzodinanphtho-(1'',7'';2,4), (7''',1''';11,13)-bisanthene	C <sub>42</sub> H <sub>18</sub>		420	320.0 <sup>b</sup> (401.0) <sup>b</sup>	60.0 (75.0)	...	16	...	...	
21.....	2,3;12,13;15,16-tribenzo terrylene	C <sub>42</sub> H <sub>22</sub>		344	340.0 (420.0)	63.0 (78.0)	...	16	...	...	
22.....	1,18;4,5;9,10;13,14-tetrabenzo heptacene	C <sub>42</sub> H <sub>22</sub>		380	270.0 (NA)	50.0 (13.0)	...	16	...	...	
23.....	1,2;3,4;5,6;7,8; 9,10;12,13-hexabenzo peropyrene	C <sub>44</sub> H <sub>20</sub>		423	150.0 (0.51)	28.0 (0.1)	...	16	...	...	
24.....	Difluoranthren-(3',5';4,6), (4'',6'';9,11)-coronene	C <sub>48</sub> H <sub>20</sub>		475	340.0 (900.0)	63.0 (170.0)	...	16	...	...	
25.....	Dicoronylene	C <sub>48</sub> H <sub>20</sub>		480	1400.0 (640.0)	260.0 (120.0)	...	16, 17	...	...	
26.....	12,13- <i>o</i> -phenylene-1,2;3,4;5,6;7,8;9,10-pentabenzo peropyrene	C <sub>48</sub> H <sub>22</sub>		447	210.0 (107.0)	40.0 (20.0)	...	16	...	...	
27.....	1,14-benzo diphenanthreno-(1'',9'';2,4), (9''',1''';11,13)-bisanthene	C <sub>50</sub> H <sub>22</sub>		411	690.0 <sup>b</sup> (680.0)	130.0 (130.0)	...	16	...	...	

NOTE.—Total *A* is the total integrated *A*-value from approximately 9000 to 14500 cm<sup>-1</sup> for molecules 1, 2, 3, 4, 5, 6, and 8–14 and from 4000 to 14500 cm<sup>-1</sup> for PAHs 15–27.

<sup>a</sup> Hirata et al. (1999).

<sup>b</sup> Total value may be slightly off, major band near detector's response limit.

REFERENCES.—(1) Hudgins & Allamandola 1995a; (2) Andrews et al. 1985; (3) Salama et al. 1994; (4) Bréchnignac & Pino 1999; (5) Hirata et al. 2003; (6) Hudgins et al. 2000; (7) Vala et al. 1994; (8) Weisman et al. 2003; (9) Hirata et al. 1999; (10) Hudgins & Allamandola 1997; (11) Hudgins & Allamandola 1995b; (12) Szczepanski et al. 1995a; (13) Szczepanski et al. 1995b; (14) Halasinski et al. 2000; (15) Ehrenfreund et al. 1992; (16) A. L. Mattioda, D. M. Hudgins, M. Bauschlicher, Jr., & L. J. Allamandola 2006, in preparation; (17) Ruiterkamp et al. 2002.

TABLE 2  
NIR BAND POSITIONS AND INTENSITIES FOR PAH CATIONS

Wavelength (nm)	Wavelength ( $\mu\text{m}$ )	Wavenumber ( $\text{cm}^{-1}$ )	$A$ ( $10^3 \text{ km mol}^{-1}$ )	Oscillator Strength ( $10^{-3}$ )	Comment
Molecule 1—Phenanthrene Cation					
1061.....	1.061	9430	0.25	0.047	...
900.3.....	0.9003	11110	11	2.1	Side bands 11070, 11150, 11190
880.7.....	0.8807	11360	vw	vw	vw
858.6.....	0.8586	11650	2.04	0.38	Side bands 11610, 11730
838.4.....	0.8384	11930	0.29	0.05	vw
820.0.....	0.8200	12200	vw	vw	vw
790.1.....	0.7901	12660	5.5	1.03	Broad band with peaks at 12420, 12490, 12570, 12780
762.7.....	0.7627	13110	vw	vw	vw
757.7.....	0.7577	13200	vw	vw	vw
Molecule 2—Fluoranthene Cation					
846.7.....	0.8467	11810	130	24	Side band 12130
744.0.....	0.7440	13440	12	2.2	...
Molecule 3—Pyrene Cation					
1041.....	1.041	9610	12	2.2	Broad band
783.1.....	0.7831	12770	8.1	1.5	...
Molecule 4—Chrysene Cation					
1168.....	1.168	8560	120	23	Shoulder 8980
1001.....	1.001	9990	37	7.03	...
878.2.....	0.8782	11390	2.05	0.39	...
674.9.....	0.6749	14820	1.4	0.26	...
Molecule 5—1,2-benz[ <i>a</i> ]anthracene Cation					
891.7.....	0.8913	11220	78	15	...
843.4.....	0.8434	11860	15	2.8	...
801.0.....	0.8010	12490	23	4.4	...

NOTES.—Molecules found in this table correspond to those in Fig. 1; vw indicates very weak bands. Band positions provided in the comments column are in wavenumbers.

TABLE 3  
NIR BAND POSITIONS AND INTENSITIES FOR PAH CATIONS

Wavelength (nm)	Wavelength ( $\mu\text{m}$ )	Wavenumber ( $\text{cm}^{-1}$ )	$A$ ( $10^3 \text{ km mol}^{-1}$ )	Oscillator Strength ( $10^{-3}$ )	Comment
Molecule 6—Tetracene Cation					
868.2.....	0.8682	11520	56	10.6	Side bands (varying strength) 11170, 11220, 11280, 11340, 11420, 11450, 11560, 11650, 11690, 11700, 11720
840.4.....	0.8404	11900	43	8.03	Side bands (varying strength) 11790, 11820, 11940
821.6.....	0.8216	12170	0.89	0.17	Side band 12130
816.9.....	0.8169	12240	1.2	0.22	...
801.8.....	0.8018	12470	7.4	1.4	Side bands 12330, 12370, 12440, 12510, 12570
774.5.....	0.7745	12910	3.2	0.60	Side bands 12730, 12800, 12950
765.9.....	0.7659	13060	3.3	0.62	Side bands
759.9.....	0.7599	13160	vw	vw	vw
745.4.....	0.7454	13420	13	2.5	...
730.9.....	0.7309	13680	2.4	0.45	Very broad and weak doublet with band 13810
Molecule 7—Benzo[ <i>a</i> ]fluoranthene Cation					
784.7.....	0.7847	12740	65	12	...
676.9.....	0.6769	14770	9.6	1.8	Uncertainty in band area due to detector range
Molecule 8—Benzo[ <i>b</i> ]fluoranthene Cation					
839.6.....	0.8396	11910	56	10.6	Side bands 11860, 12070, 12180, 12240
803.2.....	0.8032	12450	11	2.1	...
741.3.....	0.7413	13490	11	2.2	...
Molecule 9—Benzo[ <i>j</i> ]fluoranthene Cation					
1007.....	1.007	9930	vw	vw	vw
939.9.....	0.9399	10640	24	4.5	Side band 10950
823.5.....	0.8235	12140	16	3.0	...
Molecule 10—Benzo[ <i>k</i> ]fluoranthene Cation					
1051.....	1.051	9520	410	77	...
927.7.....	0.9277	10780	44	8.2	...
Molecule 11—Benzo[ <i>e</i> ]pyrene Cation					
917.8.....	0.9178	10900	18	3.3	Side bands 10380, 10700, 11110
879.0.....	0.8790	11380	0.28	0.05	...
820.3.....	0.8203	12190	7.2	1.35	Side band 11670

NOTES.—Molecules found in this table correspond to those in Fig. 2; vw—very weak band. Band positions provided in the comments column are in wavenumbers.

TABLE 4  
NIR BAND POSITIONS AND INTENSITIES FOR PAH CATIONS

Wavelength (nm)	Wavelength ( $\mu\text{m}$ )	Wavenumber ( $\text{cm}^{-1}$ )	$A$ ( $10^3 \text{ km mol}^{-1}$ )	Oscillator Strength ( $10^{-3}$ )	Comment
Molecule 12—Benzo[ <i>g,h,i</i> ]perylene Cation					
1052.....	1.052	9500	17	3.23	Side band 9430
820.3.....	0.8203	12190	1.3	0.24	...
801.1.....	0.8011	12480	1.3	0.24	...
766.1.....	0.7661	13050	12	2.16	Side band 13290, 13450
Molecule 13—Pentacene Cation					
1119.....	1.119	8940	0.14	0.026	...
1109.....	1.109	9010	0.31	0.058	...
1011.....	1.011	9890	0.85	0.16	Side bands 9920, 9950, 9990
985.2.....	0.9852	10150	9.6	1.8	Side bands 10040, 10100, 10130, 10180
954.7.....	0.9547	10470	84	15.8	Side bands 10280, 10300, 10330, 10350, 10400, 10440, 10500, 10560, 10610, 10650, 10670, 10740, 10760, 10820
917.4.....	0.9174	10900	0.57	0.11	Side bands 10850, 10880, 10930
909.1.....	0.9091	11000	0.17	0.032	Side band 11020
901.3.....	0.9013	11100	0.25	0.047	Side band 11150
879.4.....	0.8794	11370	0.25	0.047	...
842.2.....	0.8422	11870	32	6.0	Side band 11660, 11750, 12000, 12130
752.8.....	0.7528	13280	vw	vw	vw
745.8.....	0.7458	13410	vw	vw	vw
Molecule 14—Coronene Cation					
1061.....	1.061	9430	vw	vw	vw
1001.....	1.001	9990	vw	vw	vw
960.5.....	0.9605	10410	12	2.4	Side bands 10457, 10486
936.0.....	0.9360	10680	2.03	0.38	Side bands 10660, 10700, 10730, 10760
918.3.....	0.9183	10890	4.1	0.78	Side bands 10820, 10930, 10960
894.5.....	0.8945	11180	1.4	0.26	...
875.6.....	0.8756	11420	3.2	0.61	Side bands
861.0.....	0.8610	11620	2	0.37	Side bands 11690
834.2.....	0.8342	11990	4.8	0.91	Side bands 11850, 11880, 11950, 12020
801.6.....	0.8016	12480	1.9	0.35	...
791.5.....	0.7915	12640	vw	vw	vw
783.3.....	0.7833	12770	0.44	0.08	...
Molecule 15—3,4;5,6;7,8-tribenzoperopyrene Cation					
1539.....	1.539	6500	7.7	1.4	Shoulders 6280, 6740
1279.....	1.279	7820	8.1	1.5	Shoulder 8080
1001.....	1.001	9990	150	28	Shoulder 10240
863.6.....	0.8636	11580	9.5	1.8	Shoulder 11340
826.4.....	0.8264	12100	vw	vw	vw
787.5.....	0.7875	12700	8.6	1.6	Shoulder 12990

NOTES.—Molecules found in this table correspond to those in Fig. 3; vw—very weak band. Band positions provided in the comments column are in wavenumbers.

TABLE 5  
NIR BAND POSITIONS AND INTENSITIES FOR PAH CATIONS

Wavelength (nm)	Wavelength ( $\mu\text{m}$ )	Wavenumber ( $\text{cm}^{-1}$ )	<i>A</i> ( $10^3 \text{ km mol}^{-1}$ )	Oscillator Strength ( $10^{-3}$ )	Comment
Molecule 16—3,4;5,6;7,8;12,13-tetrabenzoperopyrene Cation					
2411.....	2.411	4150	vw	vw	Series of weak bands going into mid-IR
2232.....	2.232	4480	vw	vw	...
1730.....	1.730	5780	vw	vw	...
1677.....	1.677	5960	vw	vw	...
1631.....	1.631	6130	vw	vw	...
1582.....	1.582	6320	vw	vw	...
1503.....	1.503	6650	vw	vw	...
1311.....	1.311	7630	vw	vw	...
1250.....	1.250	8000	vw	vw	...
1200.....	1.200	8330	vw	vw	...
1098.....	1.098	9110	vw	vw	Shoulder to 9510 $\text{cm}^{-1}$ band
1052.....	1.052	9510	170	31	...
1022.....	1.022	9780	15	2.9	...
992.9.....	0.9929	10070	4.7	0.89	...
975.2.....	0.9752	10250	0.27	0.051	...
961.9.....	0.9619	10400	0.86	0.16	Shoulder at 10490 $\text{cm}^{-1}$
919.6.....	0.9196	10870	11	2.02	Shoulders at 10741, 10700
900.7.....	0.9007	11100	9	1.7	...
879.4.....	0.8794	11370	1	0.19	...
840.4.....	0.8404	11900	2.8	0.53	Shoulder 11770
785.1.....	0.7851	12740	3.9	0.73	Side band at 12580
743.0.....	0.7430	13460	vw	vw	...
Molecule 17—3,4;5,6;10,11;12,13-tetrabenzoperopyrene Cation					
1340.....	1.340	7460	20	3.8	...
1210.....	1.210	8260	60	11	...
1108.....	1.108	9030	13	2.5	...
1037.....	1.037	9650	8.5	1.6	Shoulder 9500
756.4.....	0.7564	13220	vw	vw	vw
705.0.....	0.7050	14180	8.3	1.6	Shoulder 140000
692.3.....	0.6923	14440	vw	vw	vw
Molecule 18—12,-13- <i>o</i> -phenylene-3,4;5,6;7,8-tribenzoterrylene Cation					
1135.....	1.135	8810	4.5	0.84	Shoulder 9100
1041.....	1.041	9600	130	24	Shoulder 9870
978.9.....	0.9789	10220	8.8	1.6	Shoulder 10390, 10480
910.6.....	0.9106	10980	6.3	0.12	Shoulder 10670, 10800
891.8.....	0.8918	11210	6.8	1.3	Shoulder 11480
842.5.....	0.8425	11870	3.8	0.71	...
794.5.....	0.7945	12590	0.39	0.073	...
776.3.....	0.7763	12880	vw	vw	vw
Molecule 19—Dipyreno-(1',3';10,2)-pyrene Cation					
1301.....	1.301	7690	140	26	Shoulders 7890, 8100, 8320, 8320, 8500, 8700, 9270
923.3.....	0.9233	10830	10	1.9	...
785.4, 769.3.....	0.7854, 0.7693	12730, 13000	15	2.8	Shoulder 12100
736.5.....	0.7365	13580	3.7	0.69	...

NOTES.—Molecules found in this table correspond to those in Fig. 4; vw—very weak band. Band positions provided in the comments column are in wavenumbers.



TABLE 6  
NIR BAND POSITIONS AND INTENSITIES FOR PAH CATIONS

Wavelength (nm)	Wavelength ( $\mu\text{m}$ )	Wavenumber ( $\text{cm}^{-1}$ )	$A$ ( $10^3 \text{ km mol}^{-1}$ )	Oscillator Strength ( $10^{-3}$ )	Comment
Molecule 20—1,14-benzodindaphtho-(1'',7'';2,4),(7''',1''';11,13)-bisanthene Cation					
1290.....	1.290	7750	vw	vw	vw
1141.....	1.141	8760	vw	vw	vw
1054.....	1.054	9490	vw	vw	vw
1008, 988.8.....	1.008, 0.9888	9920, 10110	25	4.6	Shoulders 9760, 10320
875.5.....	0.8755	11420	28	5.2	Shoulder 10870
837.0.....	0.8370	11950	5.2	0.98	...
761.5.....	0.7615	13130	3.4	0.63	...
683.6.....	0.6836	14630	260	49	Uncertainty in band area due to detector range
Molecule 21—2,3;12,13;15,16-tribenzoterrylene Cation					
1251.....	1.251	8000	45	8.4	...
1095, 1061.....	1.095, 1.061	9140, 9430	5.3	0.99	...
1000.....	1.000	10000	1.5	0.28	...
919.7.....	0.9197	10870	12	2.3	...
771.1.....	0.7711	12970	270	51	Shoulders 11640, 12160
Molecule 22—1,18;4,5;9,10;13,14-tetrabenzoheptacene Cation					
1654.....	1.654	6050	4.1	0.78	Shoulder 5740
1438.....	1.438	6950	vw	vw	vw
1079.....	1.079	9270	220	42	Shoulders 8150, 8470
938.6.....	0.9386	10650	16	3.04	...
795.1.....	0.7951	12580	1.3	0.25	...
720.9.....	0.7209	13870	23	4.4	...
Molecule 23—1,2;3,4;5,6;7,8;9,10;12,13-hexabenzoperopyrene Cation					
1256.....	1.256	7960	5.5	1.04	...
1214.....	1.214	8240	8.3	1.6	Shoulder 8360
1130.....	1.130	8850	140	25	Shoulders 8700, 8740, 9030, 8260, 9440, 9630, 10470

NOTES.—Molecules found in this table correspond to those in Fig. 5; vw—very weak band. Band positions provided in the comments column are in wavenumbers.

TABLE 7  
NIR BAND POSITIONS AND INTENSITIES FOR PAH CATIONS

Wavelength (nm)	Wavelength ( $\mu\text{m}$ )	Wavenumber ( $\text{cm}^{-1}$ )	$A$ ( $10^3 \text{ km mol}^{-1}$ )	Oscillator Strength ( $10^{-3}$ )	Comment
Molecule 24—Difluoranthren-(3',5';4,6),(4'',6'';9,11)-coronene Cation					
1887.....	1.887	5300	vw	vw	vw
1291.....	1.291	7750	330	61	Shoulders 6860, 8850
758.1.....	0.7581	13190	3.8	0.71	...
731.7.....	0.7317	13670	5.1	0.96	...
673.7.....	0.6737	14840	vw	vw	Uncertainty in band area due to detector range
Molecule 25—Dicoronylene Cation					
1816.....	1.816	5510	0.24	0.045	...
1728.....	1.728	5790	0.703	0.13	...
1415.....	1.415	7070	21	3.9	Side bands 6680, 6910, 7450, 7780
1041.....	1.041	9600	480	89	Shoulders 8710, 8870, 10970
828.8.....	0.8288	12070	5.7	1.1	...
801.2.....	0.8012	12480	2.6	0.49	...
789.5.....	0.7895	12670	0.54	0.10	...
694.1.....	0.6941	14410	870	160	...
Molecule 26—12,13- <i>o</i> -phenylene-1,2;3,4;5,6;7,8;9,10-pentabenzoperopyrene Cation					
1393.....	1.393	7180	14	2.7	Shoulders 7390, 7600
1154.....	1.154	86670	25	4.7	...
1056.....	1.056	9470	160	31	...
905.6.....	0.9056	11040	10	1.9	Doublet with 10810
Molecule 27—1,14-benzodiphenanthreno-(1'',9'';2,4),(9''',1''';11,13)-bisanthene Cation					
1333.....	1.333	7500	1.6	0.29	...
1095.....	1.095	9130	23	4.3	...
990.4.....	0.9904	10100	5.4	1.01	...
939.5.....	0.9395	10640	0.11	0.021	vw
834.0.....	0.8340	11990	38	7.1	...
704.6.....	0.7046	14190	620	117	Uncertainty in band area due to detector range

NOTES.—Molecules found in this table correspond to those in Fig. 6; vw—very weak band. Band positions provided in the comments column are in wavenumbers.

TABLE 8  
NIR BAND POSITIONS AND INTENSITIES FOR PAH ANIONS

Wavelength (nm)	Wavelength ( $\mu\text{m}$ )	Wavenumber ( $\text{cm}^{-1}$ )	$A$ ( $10^3 \text{ km mol}^{-1}$ )	Oscillator Strength ( $10^{-3}$ )	Comment
Molecule 7—Benzo[ <i>a</i> ]fluoranthene Anion					
869.3.....	0.8693	11500	9.7	1.8	...
844.8.....	0.8448	11840	vw	vw	...
814.3.....	0.8143	12280	vw	vw	...
803.0.....	0.8030	12450	0.36	0.068	...
772.7.....	0.7727	12940	5.2	0.98	...
720.1.....	0.7201	13890	2.4	0.45	...
699.2.....	0.6992	14300	7.6	1.4	...
Molecule 9—Benzo[ <i>j</i> ]fluoranthene Anion					
1077.....	1.077	9290	6.9	1.3	...
1013.....	1.013	9870	1.7	0.32	...
966.0.....	0.9660	10350	1.4	0.26	...
932.1.....	0.9321	10730	5	0.94	Doublet with 10910
751.7.....	0.7517	13300	16	3.0	...
Molecule 11—Benzo[ <i>e</i> ]pyrene Anion					
1060.....	1.060	9430	0.45	0.084	Shallow shoulder 9580
963.0.....	0.9630	10380	0.57	0.11	...
934.2.....	0.9342	10700	1.02	0.19	...
915.2.....	0.9152	10930	1.5	0.28	Doublet 10880
898.7.....	0.8987	11130	0.36	0.068	...
871.5.....	0.8715	11480	0.11	0.021	...

NOTES.—Molecules found in this table correspond to those in Fig. 2; vw—very weak band. Band positions provided in the comments section are in wavenumbers.

TABLE 9  
NIR BAND POSITIONS AND INTENSITIES FOR PAH ANIONS

Wavelength (nm)	Wavelength ( $\mu\text{m}$ )	Wavenumber ( $\text{cm}^{-1}$ )	$A$ ( $10^3 \text{ km mol}^{-1}$ )	Oscillator Strength ( $10^{-3}$ )	Comment
Molecule 15—3,4;5;6;7,8-tribenzoperopyrene Anion					
1728.....	1.728	5790	0.77	0.14	...
1160.....	1.160	8620	130	24	...
713.7.....	0.7137	14010	0.56	0.11	...

NOTES.—Molecules found in this table correspond to those in Fig. 3. Band positions provided in the comments column are in wavenumbers.

TABLE 10  
NIR BAND POSITIONS AND INTENSITIES FOR PAH ANIONS

Wavelength (nm)	Wavelength ( $\mu\text{m}$ )	Wavenumber ( $\text{cm}^{-1}$ )	$A$ ( $10^3 \text{ km mol}^{-1}$ )	Oscillator Strength ( $10^{-3}$ )	Comment
Molecule 16—3,4;5,6;7,8;12-13-tetrabenzoperoprene Anion					
1153.....	1.153	8670	11	2.1	...
1055.....	1.055	9480	5.8	1.1	Significant band area remaining after cation subtraction
982.6.....	0.9826	10180	0.3	0.056	...
866.0.....	0.8660	11550	2	0.38	...
Molecule 17—3,4;5,6;10,11;12,13-tetrabenzoperopyrene Anion					
1519.....	1.519	6580	21	3.9	Shoulder 6810
1353.....	1.353	7390	16	3.1	Shoulder 7080
1052.....	1.052	9500	1.2	0.23	...
1022.....	1.022	9780	0.22	0.041	...
899.2.....	0.8992	11120	3.05	0.57	...
826.0.....	0.8260	12110	2.7	0.51	...
Molecule 18—12,13- <i>o</i> -phenylene-3,4;5,6;7,8-tribenzoterrylene Anion					
1120.....	1.120	8930	56	10.5	...
1040.....	1.040	9610	5.8	1.1	...
1010.....	1.010	9900	0.63	0.12	...
Molecule 19—dipyreno-(1',3';10,2),(1'',3'';5,7)-pyrene Anion					
1418.....	1.418	7050	14	2.6	Doublet with 7230
1285.....	1.285	7790	32	6.0	Trailing shoulders at 8100, 8310, 8520, 8730
768.4.....	0.7684	13010	1.7	0.32	...
736.7.....	0.7367	13570	1.2	0.23	...
716.8.....	0.7168	13950	15	2.8	...

NOTES.—Molecules found in this table correspond to those in Fig. 4; vw—very weak band. Band positions provided in the comments column are in wavenumbers.

TABLE 11  
NIR BAND POSITIONS AND INTENSITIES FOR PAH ANIONS

Wavelength (nm)	Wavelength ( $\mu\text{m}$ )	Wavenumber ( $\text{cm}^{-1}$ )	$A$ ( $10^3 \text{ km mol}^{-1}$ )	Oscillator Strength ( $10^{-3}$ )	Comment
Molecule 20—1,14-benzodiazaph-(1'',7'';2,4),(7''',1''';11,13)-bisanthene Anion					
1419.8.....	1.420	7040	1.9	0.36	...
1245.....	1.245	8030	45	8.4	Side bands 7630, 7750, 7910, 8300, 8370, 8550
1142.....	1.142	8760	0.401	0.075	...
1089.....	1.089	9180	0.5	0.094	...
1067.....	1.067	9370	1.1	0.21	...
1048.....	1.048	9540	0.37	0.069	...
1041.....	1.041	9610	0.15	0.028	...
1032.....	1.032	9690	0.017	0.0032	...
1028.....	1.028	9730	0.62	0.12	...
1010.....	1.010	9900	7.4	1.4	...
991.1.....	0.9911	10090	6.4	1.2	...
959.7.....	0.9597	10420	0.204	0.038	...
889.6.....	0.8896	11240	40	7.5	...
851.2.....	0.8512	11750	2	0.38	...
840.2.....	0.8402	11900	2.4	0.45	Shoulder 11970
822.4.....	0.8224	12160	0.24	0.045	...
771.8.....	0.7718	12960	8.4	1.6	Shoulders 12910, 13030
756.1.....	0.7561	13230	0.32	0.060	...
684.8.....	0.6848	14600	280	53	Uncertainty in band area due to detector range
Molecule 21—2,3;12,13;15,16-tribenzoterylene Anion					
1260.....	1.260	7940	105	19.7	...
1161.....	1.161	8620	5.7	1.1	...
1094.....	1.094	9140	16	2.9	...
980.6.....	0.9806	10200	62	12	...
923.4.....	0.9234	10830	8.7	1.6	...
864.2.....	0.8642	11570	37	6.9	...
786.2.....	0.7862	12720	180	34	...
Molecule 22—1,18;4,5;9,10;13-14-tetrabenzoheptacene Anion					
964.8.....	0.9648	10370	67	13	Significant band area remaining after cation subtraction
Molecule 23—1,2;3,4;5,6;7,8;9,10;12,13-hexabenzoperopyrene Anion					
1151.....	1.151	8690	0.25	0.047	Band area remaining after cation subtraction
1144.....	1.144	8740	0.26	0.049	Band area remaining after cation subtraction

NOTES.—Molecules found in this table correspond to those in Fig. 5; vw—very weak band. Band positions provided in the comments column are in wavenumbers. Although it is considered a large PAH, only the NIR (0.7–1.1  $\mu\text{m}$ ) data are available for molecule 22.

TABLE 12  
NIR BAND POSITIONS AND INTENSITIES FOR PAH ANIONS

Wavelength (nm)	Wavelength ( $\mu\text{m}$ )	Wavenumber ( $\text{cm}^{-1}$ )	$A$ ( $10^3 \text{ km mol}^{-1}$ )	Oscillator Strength ( $10^{-3}$ )	Comment
Molecule 24—Difluoranthene (3',5';4,6),(4'',6'';9,11)-coronene Anion					
1797.....	1.797	5560	46	8.7	...
1468.....	1.468	6810	160	31	Side band 6320
1313.....	1.313	7620	160	30.0	...
818.5.....	0.8185	12220	3.7	0.69	...
732.2.....	0.7322	13660	520	98	...
Molecule 25—Dicoronylene Anion					
2062.....	2.062	4850	1.8	0.34	Shoulders 4790, 4750
1603.....	1.603	6240	5.7	1.1	Shoulders 5980, 6060, 6170, 6330
1555.....	1.555	6430	2.5	0.47	...
1435.....	1.435	6970	0.093	0.017	...
1347.....	1.347	7420	8.3	1.56	...
1244.....	1.244	8040	0.56	0.105	...
1147.....	1.147	8720	13	2.4	Side band to 9710
1030.....	1.030	9710	270	51	Side bands 8720, 10670
750.4.....	0.7504	13330	7.8	1.5	Shoulder to 14410
694.0.....	0.6940	14410	340	63.5	Band area remaining after cation subtraction. Includes 13330
Molecule 26—12,13- <i>o</i> -phenylene-1,2;3,4;5,6;7,8;9,10-pentabenzoperopyrene Anion					
1757.....	1.757	5690	5.2	0.98	...
1524.....	1.524	6560	0.22	0.041	...
1417.....	1.417	7060	1.04	0.20	...
1366.....	1.366	7320	0.11	0.021	...
967.4.....	0.9674	10340	1.01	19	...
Molecule 27—1,14-benzodiphenanthreno-(1'',9'';2,4),(9''',1''';11,13)-bisanthene Anion					
1333.....	1.333	7500	73	14	Shoulder 7190
1120.....	1.120	8930	40.1	7.5	...
1041.....	1.041	9610	1.9	0.36	...
902.8.....	0.9028	11080	61	12	...
737.8.....	0.7378	13550	486	91	...
677.4.....	0.6774	14760	16	3.0	...

NOTES.—Molecules found in this table correspond to those in Fig. 6; vw—very weak band. Band positions provided in the comments column are in wavenumbers.

## REFERENCES

- Aitken, D. K., & Roche, P. F. 1983, *MNRAS*, 202, 1233
- Allamandola, L. J., Greenberg, J. M., & Norman, C. A. 1979, *A&A*, 77, 66
- Allamandola, L. J., Hudgins, D. M., & Sandford, S. A. 1999, *ApJ*, 511, L115
- Allamandola, L. J., Tielens, A. G. G. M., & Barker, J. R. 1989, *ApJS*, 71, 733
- Andrews, L., & Blankenship, T. A. 1981, *J. Am. Chem. Soc.*, 103, 5977
- Andrews, L., Friedman, R. S., & Kelsall, B. J. 1985, *J. Phys. Chem.*, 89, 4016
- Bakes, E. L. O., Tielens, A. G. G. M., & Bauschlicher, C. W. 2001, *ApJ*, 556, 501
- Bauschlicher, C. W., & Langhoff, S. R. 1997, *Spectrochim. Acta A*, 53, 1225
- Biennier, L., Salama, F., Allamandola, L. J., & Scherer, J. J. 2003, *J. Chem. Phys.*, 118, 7863
- Birks, J. B. 1970, *Photophysics of Aromatic Molecules* (London: Wiley)
- Bohlin, R. C., Savage, B. D., & Drake, J. F. 1978, *ApJ*, 224, 132
- Bréchnignac, P., & Pino, T. 1999, *A&A*, 343, L49
- Cox, P., & Kessler, M. F., eds. 1999, *The Universe as Seen by ISO*, Vol. II (ESA SP-427; Noordwijk: ESA)
- Ehrenfreund, P., d'Hendecourt, L., Verstraete, L., Leger, A., Schmidt, W., & Defourneau, D. 1992, *A&A*, 259, 257
- Ehrenfreund, P., Foing, B. H., d'Hendecourt, L., Jenniskens, P., & Desert, F. X. 1995, *A&A*, 299, 213
- Haas, M. R., Davidson, J. A., & Erickson, E. F., eds. 1995, *ASP Conf. Ser. 73, Airborne Astronomy Symp. on the Galactic Ecosystem: From Gas to Stars to Dust* (San Francisco: ASP)
- Halasinski, T., Hudgins, D. M., Salama, F., Allamandola, L. J., & Bally, T. 2000, *J. Phys. Chem. A*, 104, 7484
- Hirata, S., Head-Gordon, M., Szczepanski, J., & Vala, M. 2003, *J. Phys. Chem. A*, 107, 4940
- Hirata, S., Lee, T. J., & Head-Gordon, M. 1999, *J. Chem. Phys.*, 111, 8904
- Hojtink, G. J. 1959, *Mol. Phys.*, 2, 85
- Hojtink, G. J., Velthorst, N. H., & Zandstra, P. J. 1960, *Mol. Phys.*, 3, 533
- Hony, S., van Kerckhoven, C., Peeters, E., Tielens, A. G. G. M., Hudgins, D. M., & Allamandola, L. J. 2001, *A&A*, 370, 1030
- Hudgins, D. M., & Allamandola, L. J. 1995a, *J. Phys. Chem.*, 99, 3033
- . 1995b, *J. Phys. Chem.*, 99, 8978
- . 1997, *J. Phys. Chem. A*, 101, 3472
- . 2004, in *ASP Conf. Ser. 309, Astrophysics of Dust*, ed. A. N. Witt, G. C. Clayton, & B. T. Draine (San Francisco: ASP), 665
- Hudgins, D. M., Bauschlicher, C. W., Jr., & Allamandola, L. J. 2001, *Spectrochim. Acta A*, 57, 907
- . 2005, *ApJ*, 631, in press
- Hudgins, D. M., Bauschlicher, C. W., Jr., Allamandola, L. J., & Fetzer, J. C. 2000, *J. Phys. Chem. A*, 104, 3655
- Hudgins, D. M., & Sandford, S. A. 1998, *J. Phys. Chem.*, 102, 329
- Kasha, M. 1948, *J. Opt. Soc. Am.*, 38, 1068
- Kim, H., & Saykally, R. J. 2002, *ApJS*, 143, 455
- Kjaergaard, H. G., Robinson, T. W., & Brooking, K. A. 2000, *J. Phys. Chem. A*, 104, 11297
- Lagache, G., et al. 2004, *ApJS*, 154, 112
- Li, A., & Draine, B. T. 2001, *ApJ*, 554, 778
- . 2002, *ApJ*, 572, 232
- Mattila, K., Lemke, D., Haikala, L. K., Laureijs, R. J., Leger, A., Lehtinen, K., Leinert, C., & Mezger, P. G. 1996, *A&A*, 315, L353
- Mattioda, A. L., Allamandola, L. J., & Hudgins, D. M. 2005, *ApJ*, 629, 1183
- Mattioda, A. L., Hudgins, D. M., Bauschlicher, C. W., Jr., Rosi, M., & Allamandola, L. J. 2003, *J. Phys. Chem. A*, 107, 1486
- Moutou, C., Verstraete, L., Leger, A., Sellgren, K., & Schmidt, W. 2000, *A&A*, 354, L17
- Onaka, T., Yamamura, I., Tanabe, T., Roellig, T. L., & Yuen, L. 1996, *PASJ*, 48, L59
- Oomens, J., Tielens, A. G. G. M., Sartakov, B. G., von Helden, G., & Meijer, G. 2003, *ApJ*, 591, 968
- Pech, C., Joblin, C., & Boissel, P. 2002, *A&A*, 388, 639
- Peeters, E., Hony, S., Van Kerckhoven, C., Tielens, A. G. G. M., Allamandola, L. J., Hudgins, D. M., & Bauschlicher, C. W. 2002, *A&A*, 390, 1089
- Peeters, E., Spoon, H. W. W., & Tielens, A. G. G. M. 2004, *ApJ*, 613, 986
- Puget, J. L., & Leger, A. 1989, *ARA&A*, 27, 161
- Roussel, H., et al. 2001, *A&A*, 372, 406
- Ruiterkamp, R., Halasinski, T., Salama, F., Foing, B., Allamandola, L. J., Schmidt, W., & Ehrenfreund, P. 2002, *A&A*, 390, 1153
- Salama, F., & Allamandola, L. J. 1991, *J. Chem. Phys.*, 94, 6964
- Salama, F., Bakes, E., Allamandola, L. J., & Tielens, A. G. G. M. 1996, *ApJ*, 458, 621
- Salama, F., Joblin, C., & Allamandola, L. J. 1994, *J. Chem. Phys.*, 101, 10252
- Schutte, W. A., Tielens, A. G. G. M., & Allamandola, L. J. 1993, *ApJ*, 415, 397
- Shida, T., & Iwata, S. J. 1973, *J. Am. Chem. Soc.*, 95, 3473
- Szczepanski, J., Banisaukas, J., Vala, M., Hirata, S., & Wiley, W. R. 2002, *J. Phys. Chem. A*, 106, 6935
- Szczepanski, J., Drawdy, J., Wehlburg, C., & Vala, M. 1995a, *Chem. Phys. Lett.*, 245, 539
- Szczepanski, J., Wehlburg, C., & Vala, M. 1995b, *Chem. Phys. Lett.*, 232, 221
- Uchida, K. I., Sellgren, K., & Werner, M. W. 1998, *ApJ*, 493, L109
- Uchida, K. I., Sellgren, K., Werner, M. W., & Houdashelt, M. L. 2000, *ApJ*, 530, 817
- Vala, M., Szczepanski, J., Pauzat, F., Parisel, O., Talbi, D., & Ellinger, Y. 1994, *J. Phys. Chem.*, 98, 9187
- van Kerckhoven, C., et al. 2000, *A&A*, 357, 1013
- Verstraete, L., et al. 2001, *A&A*, 372, 981
- Weisman, J. L., Lee, T. J., Salama, F., & Head-Gordon, M. 2003, *ApJ*, 587, 256